AD-A230 581

THREE DEGREES OF FREEDOM
COMPLIANT MOTION CONTROL
FOR ROBOTIC AIRCRAFT REFUELING

THESIS

Clayton M. Andersen
Captain, USAF

AFIT/GAE/ENG/90D-01

DEPARTMENT OF THE AIR FORCE
AIR UNIVERSITY
AIR FORCE INSTITUTE OF TECHNOLOGY

Wright-Patterson Air Force Base, Ohio

91 1 3 069

AFIT/GAE/ENG/90D-01

THREE DEGREES OF FREEDOM
COMPLIANT MOTION CONTROL
FOR ROBOTIC AIRCRAFT REFUELING

THESIS

Clayton M. Andersen
Captain, USAF

AFIT/GAE/ENG/90D-01

AFIT/GAE/ENG/90D-01

Three Degrees of Freedom

Compliant Motion Control

for Robotic Aircraft Refueling

THESIS

Presented to the Faculty of the School of Engineering

of the Air Force Institute of Technology
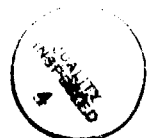
Air University

In Partial Fulfillment of the

Requirements for the Degree of

Master of Science in Aeronautical Engineering

Clayton M. Andersen, BSME

Captain, USAF

December 13, 1990

Approved for public release; distribution unlimited

Acknowledgments

The Robotic Systems Laboratory at AFIT is gifted with knowledgeable and dedicated staff and students. The Compliant Motion project would not have been possible without many dedicated people. Some like Captain Duvall were not here at the same time, but evidence of their hard work still lingers.

My thanks to Captain Leahy,'Mike', for his patience with a stubborn and sometimes slow student. I attribute a great deal of what I learned here to Mike's attitude, both in and out of the classroom. I'd also like to thank that other bald guy for his listening ear. Dan Zambon was always available to help any student with practically any kind of problem. To my colleagues in the Robotics lab, I offer my congratulations and my gratitude. Thanks for helping me keep track of reality, and for all those little problem solving sessions.

I dedicate a portion of this thesis to Wayne Wilsdon. Wayne was a great inspiration to all of his peers. He loved engineering. He was generous and always there to help a classmate. Most of all Wayne was a friend. Thanks.

I thank my lovely wife and children for allowing me to be an absentee 'everything' for the past 18 months. Without your support and love, I would have failed miserably. Finally, I thank my Father in Heaven for peace and strength.

Clayton M. Andersen

Table of Contents

List of Figures

List of Tables

AFIT/GAE/ENG/90D-01

Abstract

The Air Force Institute of Technology(AFIT) supports on-going research in application of robotic technology to enhance assembly tasks. As a testbed, AFIT supports the ground-based aerial refueling project, with an emphasis on visual servoing techniques and compliant motion control. This thesis focuses on compliant motion control. Previous research developed the testing environment, which includes a PUMA-560 industrial manipulator, and a half scale mock-up of an aerial refueling system. This effort corrected and expanded the existing two degree of freedom(DOF) compliant controller to three DOF. Three DOF compliance was demonstrated by inserting the refueling nozzle into the receiver port.Tuning, carried out by adjusting desired model variables, characterized the impedance controller to function over a wide range of desired dynamics. In addition, irregular force and velocity torque profiles were attenuated through basic filtering schemes, providing an environment in which friction compensation was tested. Finally, preliminary studies into faster trajectories provide impetus for further study in the area of high speed compliant assembly. The three DOF compliant controller combined with the visual servoing techniques, provides a strong environment to test and evaluate robotic technologies for constrained motion assembly tasks.

Three Degrees of Freedom
Compliant Motion Control
for Robotic Aircraft Refueling

I. Introduction

1.1 Motivation

One method to augment diminishing work force and protect humans from hostile environments, is the application of robotics technology to specific tasks. Some tasks currently being examined include robotic aircraft paint stripping, aircraft radiography, and canopy polishing. These applications have shown the potential of robotics to improve efficiency and reduce manpower. One of the challenges in using robotic technology for industrial and military applications, is applying only technology that has been proven for a specific scenario. This type of application requires directed and specific research along with the understanding that robots are not capable of replacing all or even most of the human applications. Yet, there are many areas where robotic technology can contribute significantly. A growing area of interest in the robotic community is constrained motion applications. Constrained motion refers to tasks performed while in contact with the environment. Humans perform most of their tasks in the constrained mode. Present generation robots perform a limited number of constrained tasks and many free space tasks. In the cases where robots perform constrained tasks, a high degree of task planning, robot training, and rigid fixturing has been implemented to accomplish the task. The reason for such efforts is that control technology for such robots is generally based on individual joint high gain proportional-derivative(PD) or proportional-integral-derivative(PID) feedback. These controllers are extremely efficient at positioning a robot at a desired point

with accuracy and repeatability. When the same controller is used for constrained tasks catastrophic results can and usually do follow.

There are many reasons humans have the ability to perform complicated constrained tasks effortlessly. These reasons can be divided into three categories: Ability to learn and recognize objects quickly; Local and global control centers; Compact and efficient sensor placement. Humans can sense and react to many things like temperature, texture, and forces. It is the ability to sense and react to forces that make human manipulation so good with constraint tasks. A simple task like inserting a peg into a hole is rather basic for humans, even in the dark. In such a task the human will touch the environment and follow it until the hole is contacted. Once initially contacted, the hand adjusts forces to allow the peg to engage and enter the hole. This type of manipulation task is often referred to as compliant motion: the ability to adjust to and surmount obstacles while performing the desired task in a stable manner. The peg-in-the-hole task is representative of a general class of assembly operations. As shown in this simple example, constrained tasks require the ability to adjust to force inputs. Therefore, for robots to perform constrained tasks in a semi- or unstructured environment, force centered control schemes combined with force sensors must be evaluated and applied. Much of the current research in robotics is involved in this area of compliant control.

The Air Force has some specific and unique areas of interest where a compliant task oriented robot may prove useful. Specifically, part sorting, automated structural analysis, parts replacement, and refueling all provide potential candidates for robotics. Each of these tasks can be dangerous and difficult for humans to perform in a chemical or hazardous environment. A robot in the same environment, if appropriately designed, would be unaffected. Currently, AFIT is evaluating aerial refueling as a testbed for applying robotics. The AFIT robotic refueling scenario is divided into two general areas: pattern recognition and compliant motion.

In the area of pattern recognition, research by Capt Shipman [40] and Capt

Bennett [7] has provided the means to find and identify the standard aircraft refueling port through digital imaging in various lighting environments. Once the port has been identified, the second area of research, constrained motion, is applied to actually insert the refueling nozzle into the receiver. Because nozzle insertion is analogous to the peg-in-the-hole task, successfully demonstrating this task provides insight into use of robotics for constrained Air Force applications.

1.2 Objective

AFIT studies in compliant motion focus on the feasibility of robotic on-ground refueling using the aerial refueling port. This method provides a potential for faster turn-around time for ground refueling. The purpose of this research effort is to improve, clarify, and expand the compliant control applications previously performed on a laboratory mock-up of the ground refueling scenario.

1.3 Problem Statement

Past research at AFIT has paved the way for a full three degree of freedom(DOF) ground refueling scenario demonstration. Captain Duvall began the work by developing the half scale mock-up of the Universal Aerial Refueling Receptacle Slipway Installation(UARRSI) port and nozzle, along with the tedious work of characterizing the basic dynamics and control laws to be used [14]. Additionally, Duvall developed the initial testbed which included computer programs integrated with a PUMA-560 serial link industrial robot, and he performed initial testing in two DOF. Captain Milholen followed Duvall's efforts by refining computer code and improving the system with the addition of a faster clock [34]. With these improvements Milholen was able to demonstrate two DOF refueling tracking and insertion.

The goal of present AFIT studies in compliant motion is to demonstrate three DOF compliant peg-in-the-hole capability by means of the ground refueling demonstration. This follow-on research effort is centered around expanding the previous

experiments from two DOF capability into the more general and useful three DOF case. At first glance, this by itself appears to be simply a minor adjustment to the previous efforts. However, the mechanism for implementing the two DOF controller contained some anomalies which needed to be characterized and corrected prior to implementing the expanded controller. In addition, Milholen recommended further improvements in friction compensation and second order model parameter selection.

The purpose of this effort is to characterize and correct anomalies in the two DOF compliant controller, expand the control to three DOF, and provide better performance through parameter selection or 'tuning' and friction compensation.

1.4 Method of Approach

The primary emphasis of this thesis was to prove and demonstrate three DOF compliant motion. The central hurdle was characterizing and correcting the anomalies from the two DOF implementation. This required a complete evaluation of the theory and subsequent computer code used to create the two DOF controller. Each of the contributing factors in the control method such as dynamics, kinematics, and force sensor integration was evaluated for theoretical and applied accuracy. Following this evaluation and the subsequent corrections, the computer code was upgraded to the three DOF form. All the two-by-two matrix equations were expanded to three-by-three arrays. Any simplifying assumptions made for the two DOF case were removed. Effectively, the inertia, mass, damping, jacobian, inverse jacobian, and jacobian transpose terms had to be recalculated then coded in their three DOF form. Once coding was completed, the algorithm was exercised using the 'effective' second order parameters which were derived from the two DOF case. Next, these parameters were adjusted within certain limiting bounds to evaluate performance changes due to this adjustment or 'tuning'.

In addition to tuning the second order model parameters, filters on force and velocity terms were applied to reduce the rough noise-type effects noticed during

the tuning process. Next, the friction model used by Milholen was included with the control law, and evaluated for effectiveness. Finally, some preliminary studies investigating the effect of increased trajectory speed on compliant motion were accomplished.

1.5 Contributions

This thesis has provided the capability to perform three DOF compliant assembly-type tasks, by demonstrating ground refueling on a UARRSI half scale mock-up. With this capability, AFIT can better assess how to apply robotic technology to Air Force issues. In addition to this significant advance, additional important contributions include:

- resolution of anomalies in the two DOF impedance control law implementation

- identification and resolution of improper force sensor coordinate frames

- characterization of impedance control robustness to wide variations in natural frequency and damping terms

- illustration of impedance control capability at much greater velocities

These capabilities provide insight for on-going Air Force research into applying robotics to support the demands of increased efficiency with a reduced work force.

1.6 Organization

This thesis is organized into six chapters. Chapter two provides a summary of the salient literature regarding force control theory and applications, including friction characteristics and effects. Chapter three identifies the test environment hardware and software. Chapter four points out the anomalies encountered and how they were corrected. Chapter five discusses the test results. Finally, chapter six concludes with summary comments and some recommendations for future research efforts in this area.

II. Literature Review

2.1 Motivation and Scope

Currently, a majority of robotic applications are centered around industrial-type control methods which are tailored to a highly fixtured environment where the manipulator remains free from the environment. Examples are spot welding and painting. In the few applications where the task is performed in contact with the environment, the contact is highly structured [22]. This style of control has limited robotics to a narrow range of applications. In order for robotics to have a more universal place in commercial and industrial applications, they must be capable of performing assembly type tasks.

Assembly is learned quickly and performed well by the human manipulator. Goto et al describe the human dextrous capability used during assembly tasks to consist of three phases [18]:

- Rough positioning; done by sight,

- Initial alignment; done by dexterity,

- Control fine motions until complete; done by delicate touch.

For robots to perform assembly tasks well, they must be capable of performing in each of the three categories of human dexterous motion, as seen in Figure 2.1.

Assembly requires the manipulator to come in contact with the environment and continue to function in a controlled accurate manner. This type of interaction with a traditional position controlled robot, produces instability. Hogan explains that contact instability is one of the reasons for so little progress in the area of robotic dextrous assembly [22].

With the increase emphasis on robotic assembly, new types of controllers have emerged which can accommodate environmental contact. Most notable are the com-
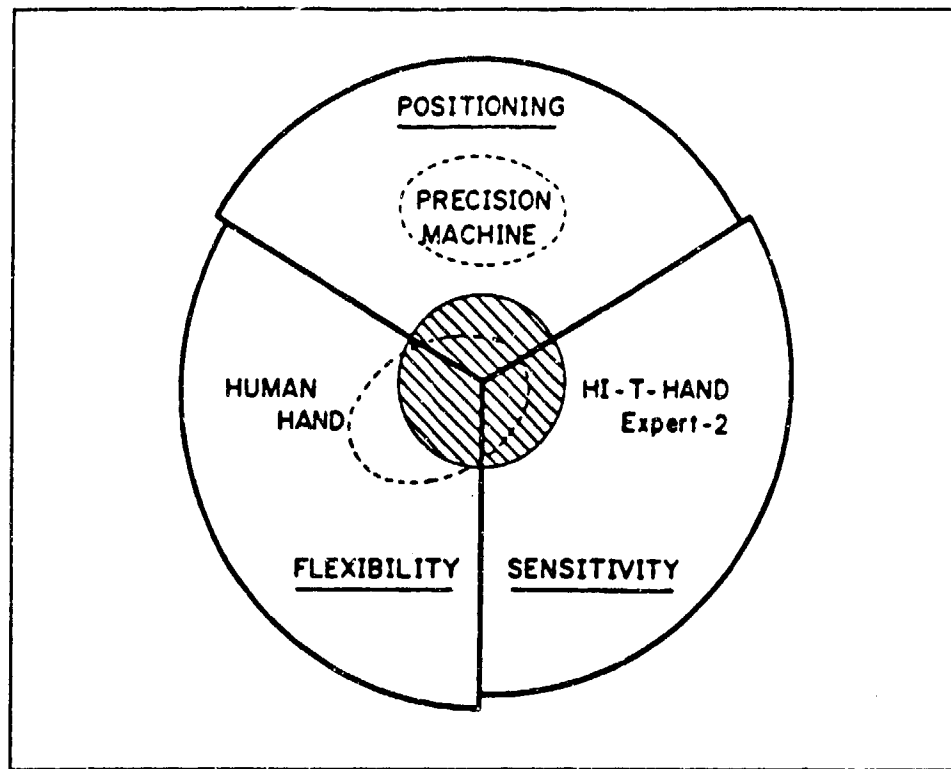
Figure 2.1. Three Functions for Assembly Tasks [18]

pliant controllers. Compliance is defined as the ability of a manipulator to adjust to constraints [37]. Compliance can be achieved in many ways which are separated into two general categories; active and passive [33]. Passive compliance deals with the flexible nature of the manipulator or the end effector. In other words, passive compliance can be designed into the physical structure of the manipulator or end effector. Active compliance is achieved through programming or controller design. Active compliance has sparked great interest because a single manipulator can be made versatile by changing its compliant nature through software or programming changes. In a passive compliance manipulator, changing to another task may require a physical restructuring of the manipulator.

Like general industry, the Air Force is interested in robotic dextrous assembly and related tasks as a means to increase efficiency and replace some tasks currently performed by humans. The purpose of this literature review is to evaluate the current

2-2

control schemes used in dextrous manipulation, and how they relate to on-going AFIT research efforts. It will focus on active compliant methods, and approaches to simplify non-linear effects such as friction and contact dynamics.

2.2 Compliant Motion Survey

Mason states that "facility in compliant motion tasks is a prerequisite to the use of manipulators in a number of new applications, namely assembly"[33]. The need to move away from the structured environment of the industrial robot is facilitated by the use of compliant control [37]. Active compliance has been studied extensively due to the flexibility it offers the user, i.e. the ability to program the same manipulator to perform under various conditions. Active compliance can be achieved in various ways. All of these depend on some form of force control. Whitney provides a detailed explanation of the various types of force control [46] . A summary is provided here.

Figure 2.2 shows a block diagram of stiffness control. This type of control converts sensed forces into position adjustments. This conversion is done through a stiffness matrix which models the total of the environment, manipulator, and sensor stiffness. Essentially this type of control models robotic environment interaction as a spring mechanism.

Damping control is similar to stiffness control, except in this case the sensed forces are converted into velocity adjustments via a damping matrix. The physical analogy for this interaction is modeling a dashpot or damper. See Figure 2.3 for the block diagram of this type of control.

In case of explicit force control, the actual trajectory is described in terms of desired force instead of positions or velocities. Forces are sensed actively and are compared to a desired force. The difference between the two forces serves as an error term to a linear force control law in this method. Figure 2.4 represents this type of controller.
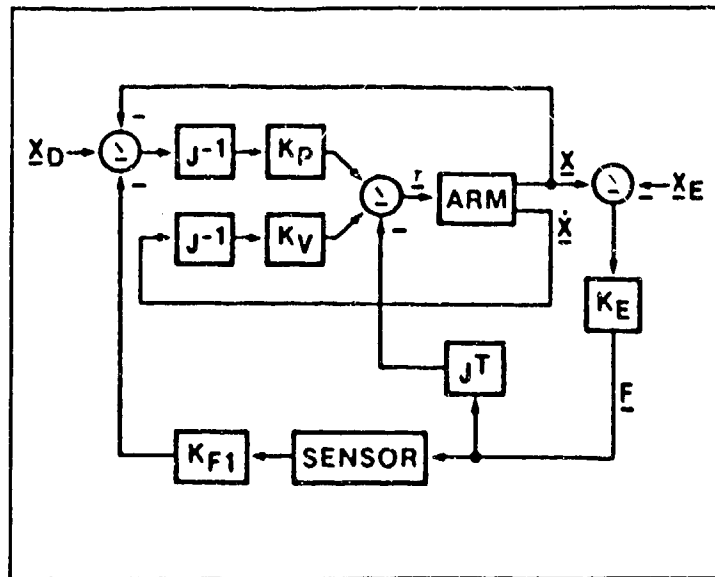
Figure 2.2. Stiffness Control [46]
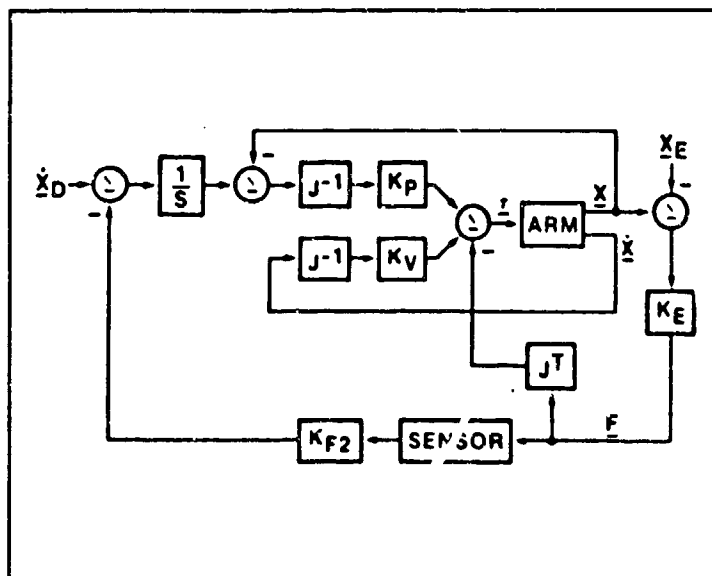
Figure 2.3. Damping Control [46]

Implicit force requires no force sensor. Displacements of the end effector and environment are converted to forces through a conversion or stiffness matrix. Figure 2.5 shows that in reality implicit force control is another form of position control. Finally, the individual joint gains are adjusted in order to obtain various manipulator stiffnesses.

Within hybrid control, position and force are controlled separately under the same control structure. First, the task is divided into constrained(contact) and unconstrained axes. Force is controlled in the constrained axes, while position is controlled in the unconstrained direction. This combination allows for high position tracking in the free space axes while simultaneously accommodating constraints in the other axes. The combination of these essentially independent controllers is made through a 'selection matrix'. The selection matrix is a diagonal n by n matrix with either one's or zero's on the diagonal. A '1' turns force control on and position control off in the corresponding axis. A typical hybrid controller is represented in Figure 2.6

Figure 2.7 portrays an impedance control scheme. Defined as a generalized summation of the stiffness and damping controllers, the impedance controller is similar to the hybrid in the sense that it combines the nature of two types of controllers. It differs in the way the combination is made. The key difference is that hybrid control functions on an either/or basis. That is, either force or position is controlled in a specific axis. Impedance control, on the other hand, regulates impedance which is a combination of force, position, and velocity terms. Note, that both stiffness and damping control can be considered subsets of impedance control. The major difference is that in the full impedance controller, both desired position and velocity trajectories are provided as inputs. In stiffness control only desired position is stated, and in damping its desired velocity.

In summary, Hogan identifies one key issue in dextrous manipulation as the ability to deal with contact instabilities. His evaluation of the various types of force
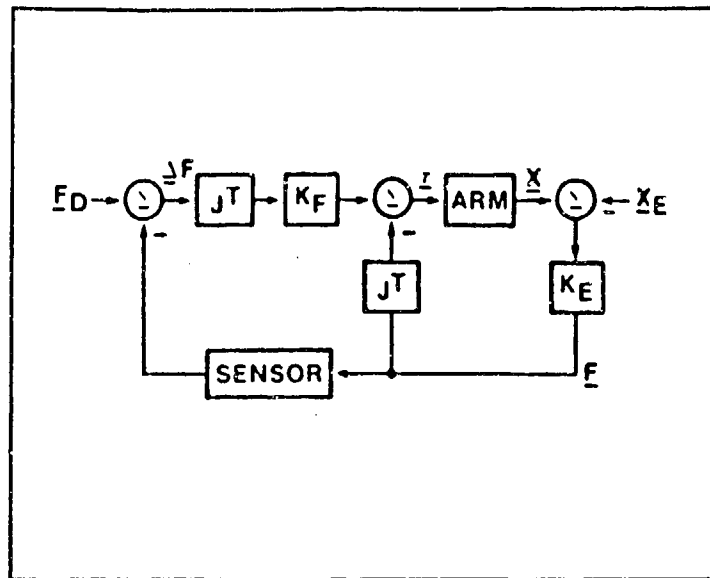
Figure 2.4. Explicit Force Control [46]
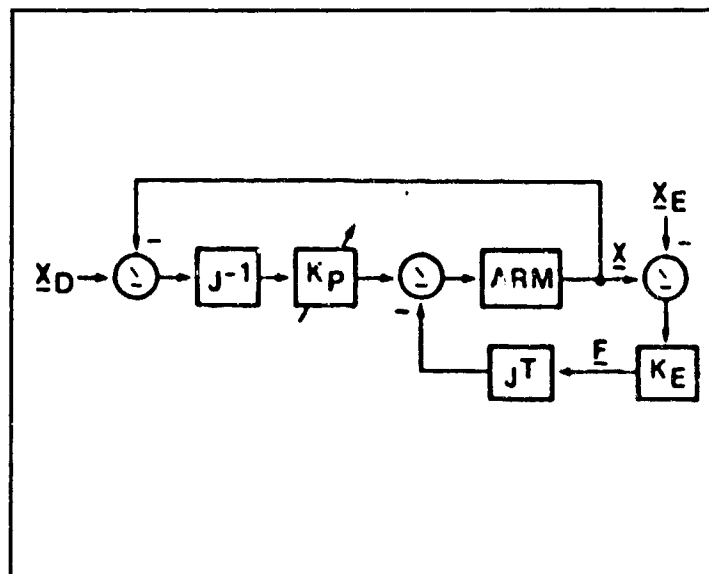
Figure 2.5. Imlicit Force Control [46]
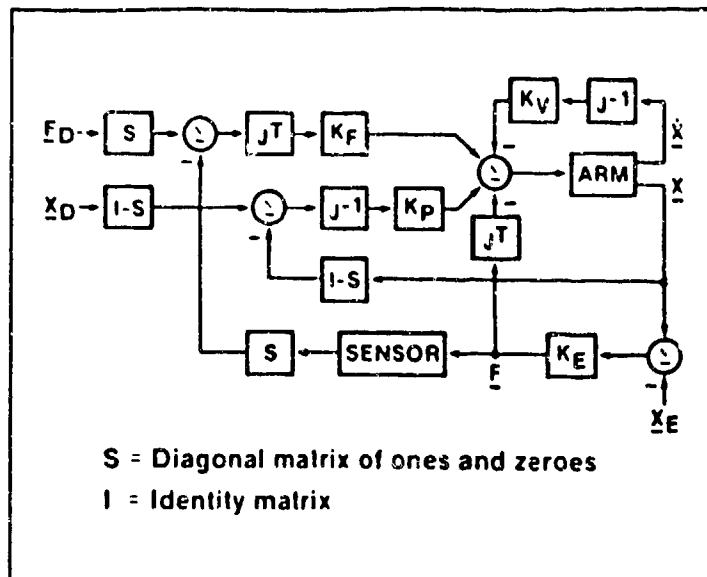
Figure 2.6. Hybrid Control [46]
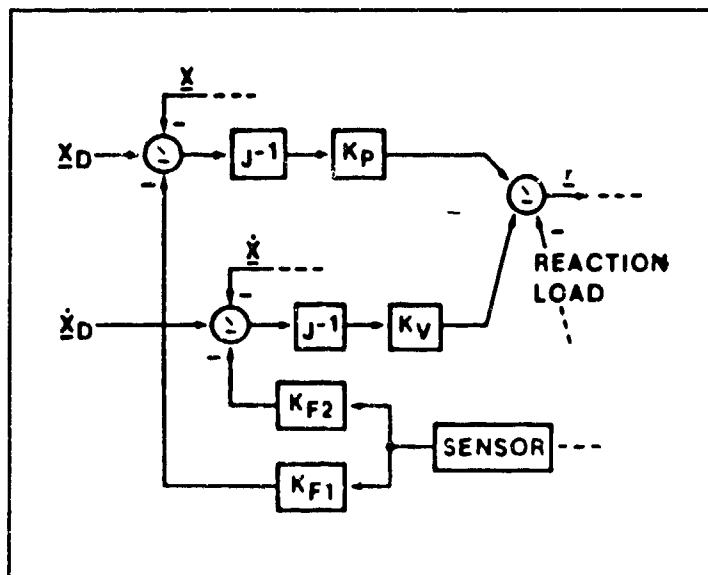
Figure 2.7. Impedance Control [46]
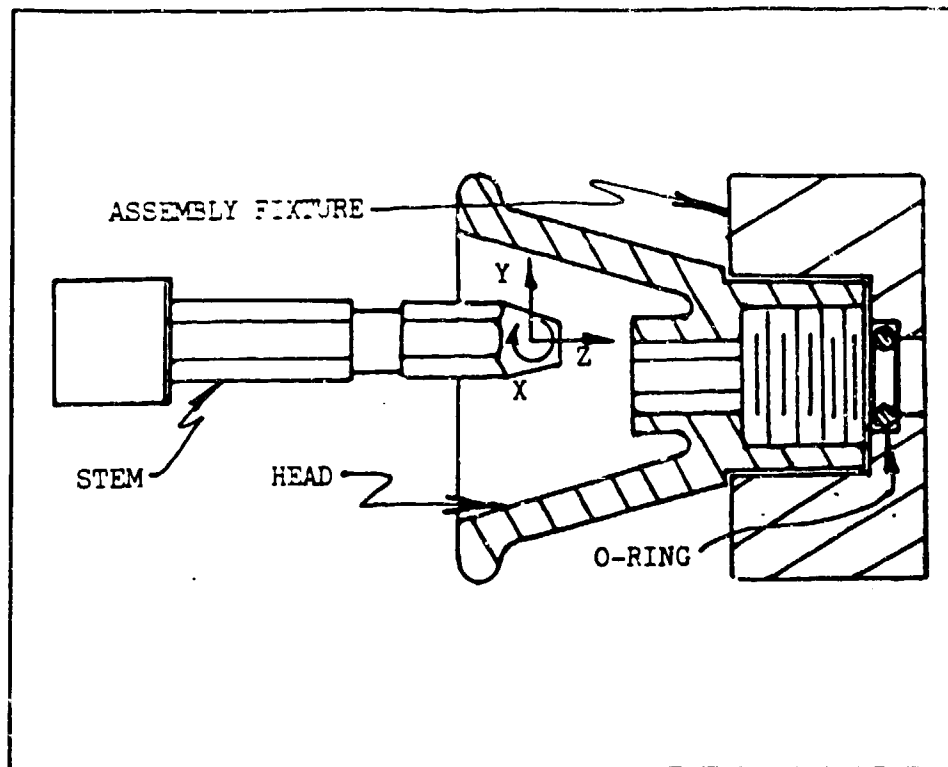
Figure 2.8. Stiffness Controlled Sprinkler Assembly [38]

control identifies that only impedance control integrates the effects of the combined or dynamic relationship between force and motion. In other words, we "must recognize that dynamic interactions are an integral part of the task" [22]. Its important to note that assembly tasks can be performed with any of the compliant control methods. Salisbury [38] used a stiffness controller to demonstrate the assembly of a lawn sprinkler assembly which is shown in Figure 2.8. However, in this example there was a degree of fixturing required to provide gross relative alignments of the mating parts.

The hybrid controller is structured in the sense that the selection matrix must be generated. This generation requires evaluation of the task being performed to determine which axes control force and position. The current focus on impedance control derives from its flexibility. Impedance control does not require exact knowledge of position or force to perform compliant tasks. In addition, this type of control

can be used in freespace. Hogan claims "the distinguishing feature and advantage of impedance control is that the same controller used to deal with free motions can also be used with real mechanical interactions"[21]. Stated another way, impedance control is the most human-like of the control schemes. Thus impedance control is an ideal candidate to perform constrained assembly tasks. The remainder of this chapter will focus specifically on impedance control.

2.3 Impedance Control

2.3.1 Theory Hogan develops impedance control using bond graph formalisms. Impedance and admittance are defined within that formalism as two types of physical system behavior. Impedances are described as elements "which accept flow (e.g.,motion) inputs and yield effort (e.g.,force)." Admittances are the inverse, that is, elements "which accept effort (e.g.,force) inputs and yields flow (e.g.,motion)." A physical example of impedance and admittance is a spring and mass, respectively.

Admittance and impedance are common concepts in linear electrical theory [19]. In that context the two concepts are essentially reciprocals of each other. However, in manipulation tasks they are generally non-linear, non reciprocal in nature. Basically, Hogan's formalization determines that certain physical elements are inherently admittances or impedances. The foregoing descriptions are important in impedance control development because the nature of interaction between elements is determined by their inherent behavior. "The most important consequence of dynamic interaction between two physical systems is that one must compliment the other"[19]. Therefore, when two systems interact they must be compliments; if one is an admittance the other must be an impedance. This is similar to the impedance matching necessary between an amplifier and a speaker.

Masses are inherently admittances. Constrained robotic tasks create the situation in which two masses interface; the robot and the environment. As previously stated, for physical systems to interact in a stable manner they must be compliments
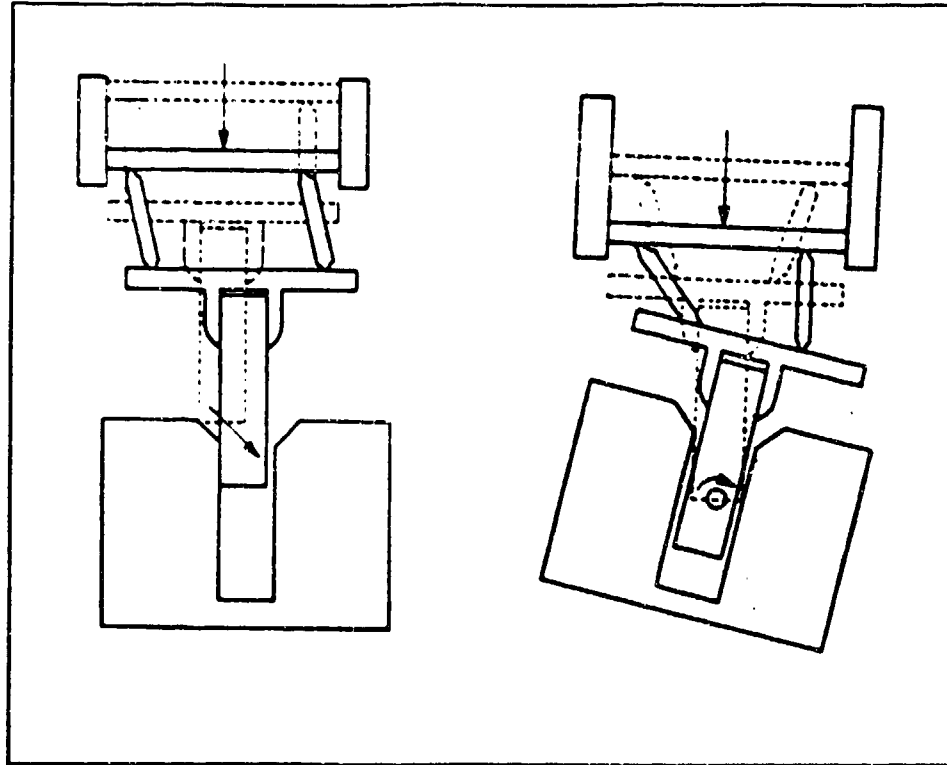
Figure 2.9. RCC Graphical Example [25]

i.e., if one interacting element is an admittance, the other must be or perform like an impedance. To achieve this, there are three options: cause the environment to emulate an impedance; add a third impedance element at the interface or; cause the manipulator to emulate an impedance. Generally speaking, the environment is not easily modified to emulate an impedance. This shifts the focus to one of the other two options. Introducing a third interfacing element with impedance characteristics is one motivation for passive compliant devices such as the Remote Center of Compliance shown in Figure 2.9, or the soft sensor.

However, these methods have limited applications and performance regions [19]. The final choice is to require the manipulator to emulate an impedance. Due to the programmable nature of robotic controllers, this option is given the designation of impedance controller [19].

The foundation for Hogan's approach to impedance control is to model the

manipulator as a second order spring-mass-damper system. Such a modeling provides all the essential elements necessary to emulate a wide range of impedance values. The spring portion provides necessary position/tracking control. The damper provides damping through velocity terms. Finally, the mass provides the essential capability to modulate force terms [21].

2.3.2 Controller Implementation Hogan's analysis of impedance control resulted in the following general control law [20]:

$$\tau_{act} = I(q)J^{-1}M^{-1}K[x_0 - L(q)] + S(q)$$
$$+ I(q)J^{-1}M^{-1}B[v_0 - J\dot{q}] + V(\dot{q})$$
$$- [J^T + I(q)J^{-1}M^{-1}]F_{int}$$
$$- I(q)J^{-1}G(q,\dot{q}) + C(q,\dot{q}) \tag{2.1}$$

The control law subsequently implemented by Duvall [14] was

$$\tau_{act} = I(q)J^{-1}M^{-1}K[x_0 - L(q)] + S(q)$$
$$- I(q)J^{-1}M^{-1}BJ\dot{q} + V(\dot{q})$$
$$- [J^T + I(q)J^{-1}M^{-1}]F_{int} \tag{2.2}$$

Finally, the control law implemented by Milholen [34] was

$$\tau_{act} = I(q)J^{-1}M^{-1}K[x_0 - L(q)] + S(q)$$
$$+ I(q)J^{-1}M^{-1}B[v_0 - J\dot{q}] + V(\dot{q})$$
$$- [J^T + I(q)J^{-1}M^{-1}]F_{int} \tag{2.3}$$

where:

q is the measured joint position

$\dot{q}$ is the computed joint velocities

I is the manipulator inertia matrix

J^{-1} is the inverse jacobian matrix

M^{-1} is the inverse desired mass matrix

K is the desired stiffness matrix

x_0 is the commanded position

L is the position from forward kinematics

S is the gravity compensation term

B is the desired damping matrix

v_0 is the commanded velocity

V is the friction compensation

J^T is the jacobian transpose

F_{int} is the interface force between constraint and manipulator

G and C are coriolis and centripetal terms

Equations 2.1, 2.2 and 2.3 are divided into position dependent terms on the first line, velocity dependent terms on the second line, and force related terms on the third line. Duvall's implementation of Hogan's law assumes that the non-linear terms, Coriolis and centripetal, are approximately zero. Duvall also assumed that the commanded velocity was zero. Milholen's version of Equation 2.1 implements a non-zero commanded velocity term. The control law implemented in this effort was a three by three matrix version of Equation 2.3.

2.4   Issues in Impedance Control

The ability to perform constrained motion makes impedance control widely studied. At the same time, constrained motion is a source of some difficult problems.

Stability is a concern whenever force sensors are included in a system [36, 47] and the influence of unmodeled, non-linear effects such as friction and other mechanical joint interactions are difficult to model and compensate.

2.4.1 Stability Sharon and others [39] defined a technique termed physical equivalence which originates from Hogan's discussion on impedance control. Physical equivalence states that a controlled physical system can be made equivalent to another uncontrolled physical system [19]. Based on physical equivalence, Sharon et al. propose that to obtain stability in a controlled physical system, merely require that the target system emulate another known stable system. The example they use is a stable spring-mass-damper configuration. Therefore, if a manipulator is modeled and controlled to emulate a spring-mass-damper, it will be stable as well. This is the same reasoning used by Hogan to develop the impedance control law. Hogan [19] and others [3] discuss that the mass term is the key to determining contact stability. Thus the spring and damper terms provide for minimum error tracking, while the mass term governs contact stability.

2.4.2 Non-Linear Effects Perhaps the limiting factor in the physical equivalence method, is controlling the system such that it truly behaves like the desired model. The realities of phenomena such as friction, gear backlash, and non-linear dynamics may severely limit how well the controller causes the system to emulate the desired behavior. Salisbury noted that coulomb friction in manipulator joints is the most severe non-linearity involved in manipulation [38] . A separate discussion of friction, including coulomb, follows the discussions on backlash and dynamics.

2.4.2.1 Backlash Tustin described backlash as the effect caused while "the displacement of one mechanical part produces equal displacement in another mechanical part, but only after taking up a definite clearance in the direction of drive" [44]. Tustin further stated that backlash has little effect on a system when

displacements are much greater than the backlash magnitude. However, when displacements are not much larger than backlash magnitude, the result can be a phase lag of 90 degrees or greater. This phase lag can contribute to instabilities [44]. When the axis of rotation for a joint is perpendicular to the gravity field the backlash effects are dramatically reduced or eliminated [27]. This is demonstrated in the large joints of the PUMA 560 manipulator. The axis of rotation for Joint one is co-linear with the gravity field, while the axes of rotation for joints two and three are perpendicular to that field. Ahmad notes that backlash is generally prominent only in joint one of the PUMA 560 [1]. One approach used to eliminate backlash effects is to employ direct-drive methods. Another is to design anti-backlash mechanisms into the manipulator. This type of anti-backlash technique is functional on the particular PUMA used in this research.

2.4.2.2 Dynamics: Coriolis and Centripetal These dynamics are nonlinear terms that are velocity and position dependent. The coupling effects of Coriolis and centripetal terms are more pronounced as velocity increases. To minimize design complexity, these terms are often either ignored or linearized. Leahy et. al have shown that feedforward and other model-based dynamic compensation techniques which include these terms can greatly improve tracking performance [28, 30]. In some cases, if velocity is small, the Coriolis and centripetal terms can be ignored with good results. Duvall [14] and Milholen [34] use this approach in their evaluation because constrained tasks are generally performed at slow speeds.

2.5 Friction

Friction is an element in nearly all mechanical systems [8, 13] , yet it is extremely difficult to model owing to its discontinuous and non-linear nature [13, 4, 17, 43]. One of the complicated aspects of friction is that it is manifest at various levels, from lubricant effects [5] to material deformations [5, 45]. Of all the various ways to categorize frictional effects, the most common are coulomb, stiction, and viscous.

Many research efforts have identified friction as the cause or a major contributor to undesirable performance such as limit cycles and stick-slip motion [10, 43, 44, 5, 13]. The remainder of this section will evaluate the effects of the various categories of friction on system performance.

2.5.1 Coulomb Friction is defined as a "dissipative force that appears at the contact surface of two bodies in relative motion" [17]. This type of friction results in a force that always opposes the direction of motion. Compensating for coulomb friction can require up to 25 percent of total motor torque [17]. Instead of a singular quantity, coulomb friction is a summary description of many complicated interactions that occur at a lower level [17, 9, 45]. This is perhaps the central reason that compensating for friction effects is difficult [10, 13]. Another contributing factor to the complexity of coulomb friction is the discontinuity at zero velocity [43].

2.5.2 Static Friction Static friction deals with bodies at rest. When an external force is applied to a body at rest, static friction will produce a nullifying counter force in order to keep the body at rest. This force continues until the external force reaches a threshold above which motion occurs. Similar to coulomb friction, static is discontinuous at zero velocity [43]. Often, this type of friction is combined with stiction [43, 13].

2.5.3 Stiction Stiction is defined as that portion of static friction force which is greater than the magnitude of coulomb friction force [10, 8, 45]. Associated with stiction is a concept called break-away. Break-away force is the point at which static friction forces can no longer oppose the applied forces, allowing for object motion [9, 43]

2.5.4 Viscous Friction Viscous friction is associated with the viscous nature of lubricants used in machine parts [5]. Generally, this effect increases linearly with increases in velocity.

2.5.5 Effects of Friction Friction is present to some degree in all mechanical systems. In evaluating the literature, a common theme emerges: Inexact friction compensation can degrade performance. For example, overcompensation of coulomb friction can lead to unstable limit cycles [10, 9]. Another result of inexact compensation is phase shifts that can actually amplify rather than reduce the negative effects of friction [44, 43].

Predominance of one type of friction over another depends largely on the velocity involved. Research shows that at low velocities, coulomb and static friction dominate due to the non-linear, discontinuous nature in that range [5, 13, 43, 44, 16]. Currently, many of the force control tasks are accomplished in this low velocity range [24, 18, 43, 34, 14]. As a result, there is a heavy emphasis on ways to reduce or eliminate coulomb and static friction effects.

2.6 Friction Compensation

There are various methods used to minimize or zero the effects of friction on a system. The major contributions to compensation techniques are modeling and adaptation. This section will review the current efforts using these tools to reduce or eliminate friction influence.

For any given system, the level of performance will dictate the fidelity of the model used to represent that system. Generally, " due to the complexity of friction models in individual components, robotics researchers typically consider an aggregate friction model for each robot joint" [13]. If implemented correctly, modeling serves to linearize, reduce, or eliminate frictional effects. Feedforward terms such as those in model-based control [31] are one example of how modeling can linearize non-linear effects [8]. Obviously, the more accurate the model, the more nullifying the compensation [45]. Unfortunately, exact models are not feasible nor available, due to the complex nature of friction in physical systems. The most common form of friction models are variants of an aggregate coulomb and stiction model. Some
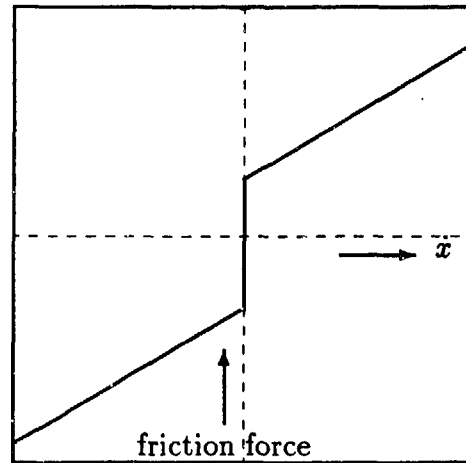
Figure 2.10. Composite Friction Model [34]

friction models are piece-wise linear combinations of coulomb and stiction, while others include the effects of Tustin's [44] exponential decay to transition between static and coulomb terms [8]. Still other models combine viscous friction with one or more of the above mentioned models [34, 29, 13]. Figure 2.10 shows the model used by Milholen [34].

One technique used to avoid overcompensation is to establish maximum values needed to fully compensate for a particular term. Once the maximum is established, the actual compensation term is set at a value less than the maximum. In this way, unstable limit cycles resulting from coulomb overcompensation can be avoided [29, 34]. Adaption techniques have been given more attention as methods to deal with inexact modeling. Many researchers working on friction models have concluded that adaptive techniques offer the greatest general method to reduce or nearly eliminate the effects of friction [8, 9, 10, 4, 16, 42]. Adaption techniques are treated only briefly in this effort. They appear to be a logical next-step area for future research following the successful implementation of the three DOF control scheme with a traditional friction model.

2.7 Summary

This chapter has reviewed the motivation for using compliant motion force control to develop robotic refueling. The use of impedance control by Duvall [14] and Milholen [34] has shown that this type of force control is well suited for the peg-in-the-hole assembly task represented by aircraft refueling. Refueling, and other slow velocity assembly tasks introduce problems such as the dominance of frictional effects. Combining the inherently unstable aspect of force control with slow velocities, creates the need for methods to counter these effects. The literature revealed that modification of the mass term in the impedance controller can eliminate the unstable force control. Friction effects can be reduced through appropriate modeling and/or combined with the emerging adaptive approaches. The next chapter will examine the implementation of these ideas in aircraft refueling.

III. Tools and Implementation of Impedance Control

3.1 Overview

This effort is an expansion and clarification of the work done by Milholen [34]. In order to fully understand the results, its necessary to describe the test environment used to create the data. Most of the equipment and theory used to create the three degree of freedom impedance controlled robotic refueler remains unchanged from that used by Duvall [14] and Milholen [34]. This chapter will describe the following aspects of the test environment: hardware, system support software and, control algorithm.

3.2 Hardware

The hardware used is separated into functional categories defined by the AFIT Hierarchical Control System (AHCS) implemented by Duvall and enhanced by Milholen. The central concept behind this system is to utilize hardware at levels best suited for specific tasks. This system is divided into three levels: organizer, coordinator, and hardware. Duvall [14:4-17] and Milholen [34:3-7] provide a more complete description of the various levels. Figure 3.1 provides a graphical portrayal of the AHCS, with a description to follow.

3.2.1 Organizer
The organizer level facilitates user interface, handles communication protocols with the coordinator, provides the capability to execute large off-line calculations, and maintains safety functions for the system. Currently, AHCS accesses one of two available VAXstation III computers for use at the organizer level.

3.2.2 Coordinator
This level is the key portion of the AHCS. It provides the link between the organizer and hardware levels. This includes communicating with the manipulator and the force sensor. Milholen [34:3-7] states that this level is used
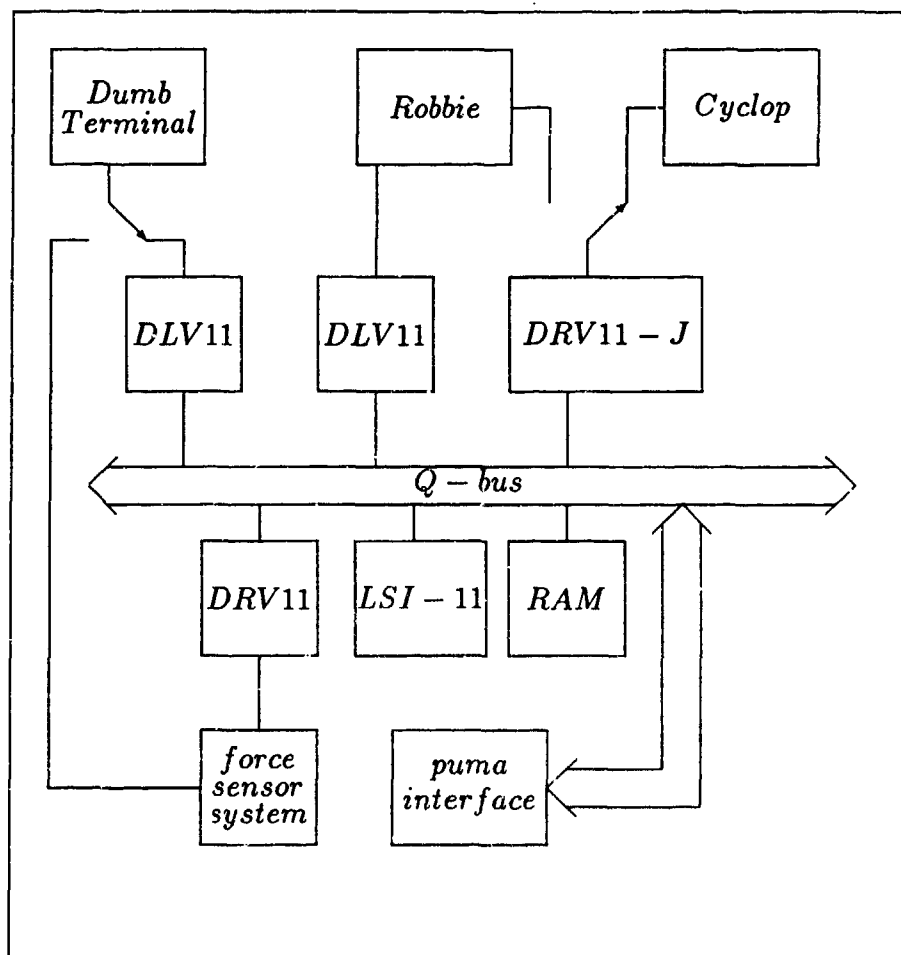
Figure 3.1. Hierarchial Control System [34]. Robbie and Cyclop are both VAXStation IIIs.

to collect and partially process data from the manipulator and force sensor and control communication tasks. The hardware at this level is the PUMA LSI-11/73 along with RAM, and various communication devices connected through a Q-bus.

3.2.3 Experimental Hardware The target of the AHCS operating hardware is at this level. Here is where the manipulator and the force sensor electronics reside. These provide the means to perform the desired experimentation.

PUMA robot arm link coordinate parameters					
Joint i	θ_i	α_i	a_i	d_i	Joint range
1	90	-90	0	0	-160 to +160
2	0	0	431.8 mm	149.39 mm	-225 to 45
3	90	90	-20.32 mm	0	-45 to 225
4	0	-90	0	433.07 mm	-110 to 170
5	0	90	0	0	-100 to 100
6	0	0	0	56.25 mm	-266 to 266
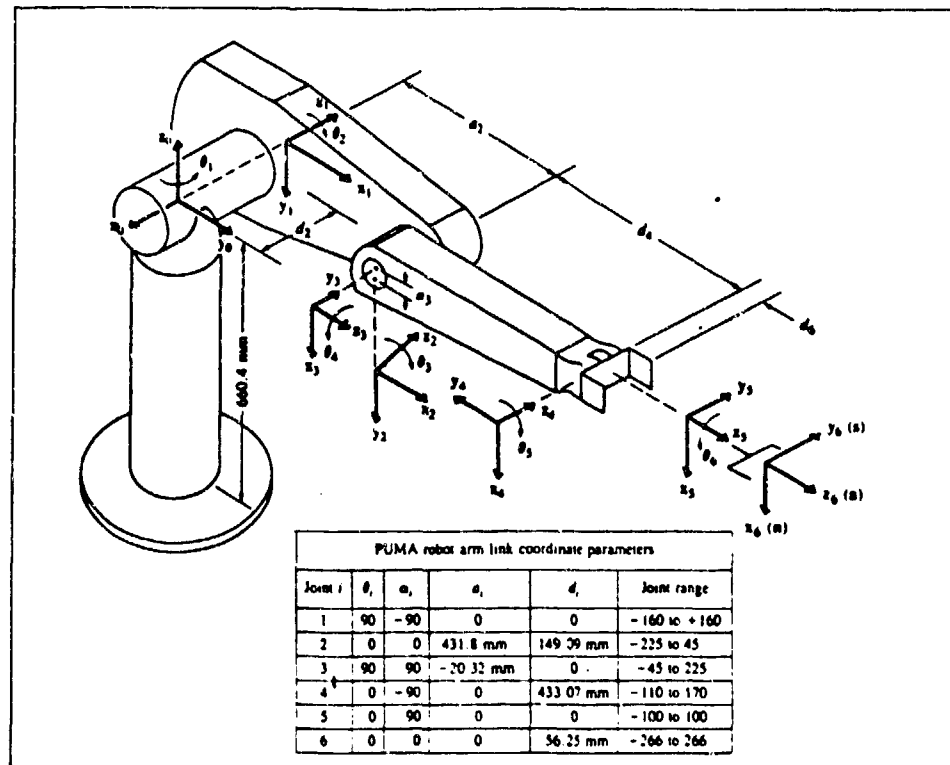
Figure 3.2. PUMA-560 Manipulator with DH Coordinate Frames [15]

3.2.3.1 Manipulator The manipulator used was a PUMA 560. This robot is an industrial-type six degree of freedom vertically articulated manipulator. It provides a good framework for evaluating various performance characteristics. Figure 3.2 represents the PUMA 560 manipulator along with the Denavit-Hartenburg(DH) coordinate frames. The manipulator derives three DOF from the three heavy links. The remaining three DOF are contained in the roll-bend-roll wrist. This research applied the compliant controller to the degrees of freedom associated with the three heavy links of the PUMA. The wrist was commanded by a traditional PD control law that forced the wrist to remain rigid.

3.2.3.2 Force Sensor The force sensor provides for six axis force monitoring. This particular force sensor was manufactured by JR³ Incorporated. The sensor package includes the transducer, support electronics, and power supply. Fig-
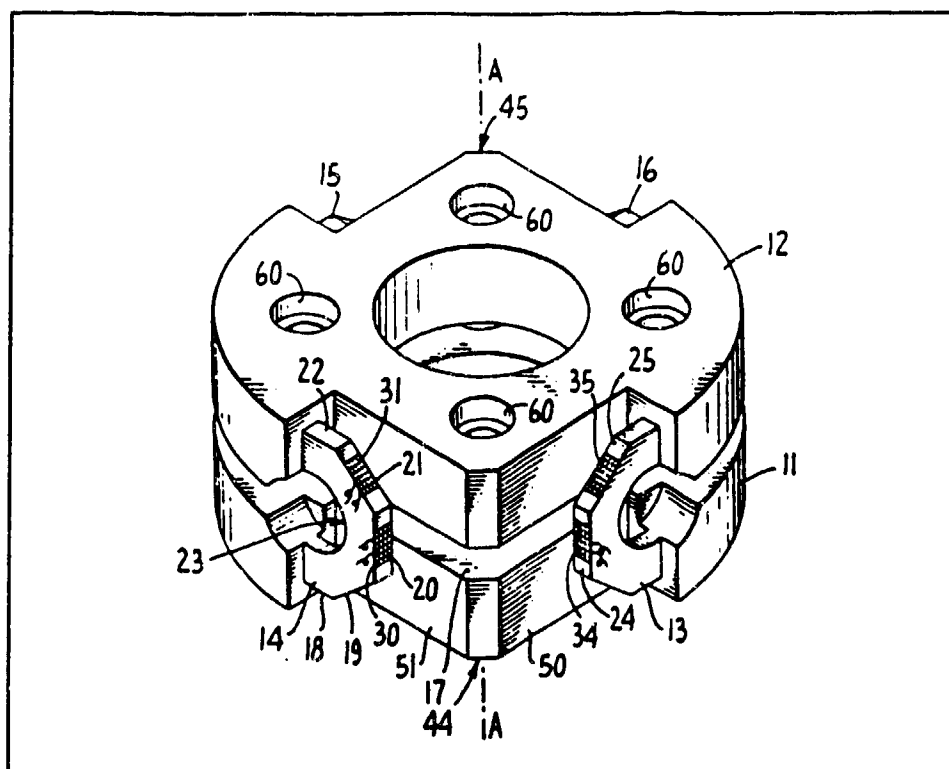
Figure 3.3. JR3 Force Transducer [46]

ure 3.1 shows the integration of the sensor package into the test environment. The transducer shown in Figure 3.3 consists of

> two parallel plates connected by four octagonal 'bridges'. The plates are bolted separately to the PUMA and the tool, so all load must pass through the bridges. Foil strain gages are mounted on the sides of the octagons, and resistance changes in the strain gauges are measured and interpreted as forces or moments using a calibration matrix unique to each transducer [14:4-8].

In figure 3.3, the bridges are represented by numbers 15, 16, 22, and 25. The strain gages are the checkered patterns shown on the bridges. The transducer is attached to the tool mounting plate on the PUMA joint six. The support electronics are housed separately from any other hardware. The electronics are divided into two pieces: the power supply, and active electronics. The active electronics provide the sensor operating system. This operating system allows for calibration, and system

diagnostic checks, and communication with other systems. For this research, all real-time data transfer occurs via a DRV-11 parallel interface. Sensor calibrations and bias removal are accounted for in the FARCADE program software.

3.2.3.3 Refueling Port To demonstrate refueling type tasks, a half-scale model of a standard UARRSI was designed by Duvall and fabricated in the AFIT model shop [14]. The mockup consists of two major parts: the slipway, and the refueling boom nozzle. The slipway is an approximate representation of an actual slipway. In a UARRSI slipway there is a smooth transition from the open slope to the receiver. Duvall chose to make the fabrication easier by making the transition a squared corner. This modification does not affect the ability to simulate compliant refueling tasks. It does create a test environment which presents a more severe obstacle to surmount. In actuality, this design provides a means to test compliance techniques at extreme path discontinuities. Attached to the force sensor transducer, the nozzle consists of three parts that are threaded together: the mounting plate, the shaft, and the nozzle end. The nozzle portion is only representative of an actual nozzle in the diametral dimensions. Capt Duvall essentially fabricated a 'soup can' which threads onto the end of the shaft. As with the port, this simplifying change in no way diminishes the ability to examine compliant tasks. This experiment made one slight modification to Duvall's nozzle design. Duvall used a three portion threaded shaft to facilitate various applied moments by changing the shaft length. This application was never used however due to clearance problems between the PUMA and the slipway The threaded shaft failed under heavy test loads. Therefore, a solid shaft of like specifications was fabricated for this thesis.

3.3 System Support Software

The software used in this thesis is based on the previously mentioned hierarchical concepts. At the AFIT robotics lab, a general test environment is used to evaluate various control laws. To facilitate this general nature, a software environ-

ment was created by previous researchers. This environment is termed the AFIT Robotic Control Algorithm Development Environment (ARCADE) [32, 26, 14, 34]. ARCADE is the software side to the AHCS. Here programming languages are used where most appropriate, i. e. the high level language FORTRAN is used at the organizer level on the VAXstations. At the coordinator level, PDP assembly language is used for speed and compactness. ARCADE also provides ability to access various control schemes and apply them to different manipulators. FARCADE, a derivative ARCADE, was created by Capt Duvall [14] and subsequently modified by Capt Milholen [34]. The 'F' represents 'force'.

Capt Duvall had limited computer resources available and was restricted to implement extensive assembly language code at the coordinator level [14]. With more abundant computer resources, Capt Milholen reorganized much of the taskings. Much of the assembly code at the coordinator level was re-hosted in VMS FORTRAN and applied at the organizer level. Milholen's effort allowed for only essential functions at the coordinator, and provided a better user interface by moving much of the tasks to the organizer. No structural changes were made to Milholen's FARCADE during this effort.

3.3.1 FORTRAN Support There are many support sub-programs called by FARCADE. They vary from loading data files containing PUMA and force sensor constants, to creating actual cartesian trajectory files, and data handling options like graphing and storage.

3.3.2 Assembly Language Support There are a number of PDP-11 assembly code programs that support the FARCADE environment. The most important one is the Servo Data Concentrator ANGLES and FORCE (SDCAAF). It provides the vital link between the PUMA and the user by collecting and shuttling joint angles, motor currents, and forces from the force sensor between the hardware and organizer level. The assembly sub-program that actually interfaces with the force sensor is

called GETRFV. Some of the key FORTRAN sub-programs will be discussed in the Section 3.5.

3.4 Control Algorithm Development

The control law use in FARCADE is based on Hogan's impedance control law. As stated in chapter two, impedance control causes the manipulator to behave like an impedance. This impedance controller models the manipulator as a spring-mass-damper. The exact values are arbitrary so long as certain ratios of these terms are maintained. This modeling is referred to as the "desired dynamics" model by Hogan [19, 34]. The development of this control law is presented next.

3.4.1 Impedance Controller
This subsection presents a condensed version of the development done by Duvall [14:p 3-6, appendix A] and modified by Milholen [34:p 3-16]. Figure 3.4 displays a block diagram of the controller described below.

Beginning with the desired dynamics concept, the mathematical representation is found in Equation 3.1 where 'x' and 'v' represent cartesian position and velocity respectively, and the subscripts 'a' and 'd' represent actual and desired values.

$$F_{int} = K(x_d - x_a) + B(v_d - v_a) + M\frac{dv}{dt} \qquad (3.1)$$

This is a matrix equation which can be implemented up the number of DOF of the manipulator involved; six for the PUMA. Because the M, B, and K matrices are each diagonal, these equations can be analyze as decoupled linear second order equations. Duvall and Milholen implemented only two DOF involving joints two and three. These equate to the world x-z coordinate plane. One of the major contributions of this thesis was to upgrade the controller to three DOF, which is general enough to demonstrate robotic refueling for a wide class of applications. Noting that the difference terms in Equation 3.1 are simply error terms of the form of Equation 3.2
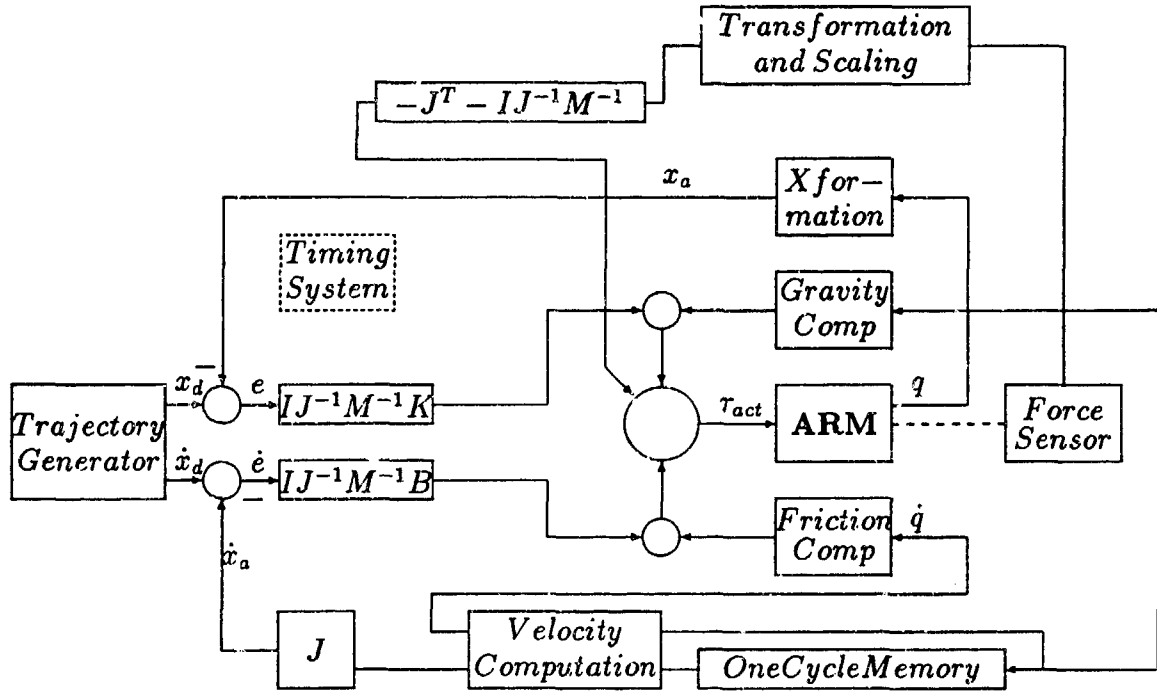
Figure 3.4. Control System in Block Diagram Form. [34]

where 'a' represents cartesian acceleration,

$$e = x_d - x_a$$

$$\dot{e} = v_d - v_a$$

$$\ddot{e} = a_d - a_a \tag{3.2}$$

Equation 3.1 can be re-written as:

$$F_{int} = Ke + B\dot{e} + M\ddot{e} \tag{3.3}$$

Applying a Laplace transform to Equation 3.3 we obtain the the following transfer function:

$$\frac{E(s)}{F_{int}(s)} = \frac{1}{s^2 + \frac{B}{M}s + \frac{K}{M}}$$ (3.4)

Equating the characteristic polynomial from Equation 3.4 with the characteristic equation for a second order system,

$$s^2 + 2\zeta\omega_n s + \omega_n^2 = s^2 + \frac{B}{M}s + \frac{K}{M}$$ (3.5)

We obtain the following relationships:

$$2\zeta\omega_n = \frac{B}{M}$$
$$\omega_n^2 = \frac{K}{M}$$ (3.6)

From pole placement techniques [11] the two closed-loop poles are the following:

$$s = \underbrace{-\zeta\omega_n}_{1} \pm j \underbrace{\omega_n\sqrt{1-\zeta^2}}_{2}$$ (3.7)

where underbrace '1' represents σ and underbrace '2' represents ω_d. The exact values for B, K, and M are specified such that the relationships to ζ, ω_d, and ω_n are maintained. Like Duvall [14] and Milholen [34], ζ was initially chosen to be greater than one to facilitate over-damping. The choice for ω_n is determined based on other techniques that will be discussed in Chapter Four. By specifying ζ and ω_n the bounds are set for the choices of desired mass (M), damping (D), and spring constant or gain (K). Within these bounds the specific values can be adjusted to meet the particular contact scenario encountered. This provides a simple method for tuning based on different impedance/admittance values encountered at the manipulator interface.

To fully implement the control law it's necessary to include other terms that allow for complete controller function in cartesian space. These terms account for

the physical nature of any manipulator: inertia due to the mass, gravity and friction, and the kinematic relationship of all points in the manipulator. The following subsections detail these items.

3.4.2 Dynamics Reference [15:p 84-98] provides an in-depth discussion of dynamic terms. A brief summary of that work is provided here. By applying energy equations of the Lagrange-Euler formulation to a robot manipulator, the generic equation of motion reduces to the matrix equation [15]:

$$\tau(t) = \mathbf{I} \ (\mathbf{q}(t))\ddot{\mathbf{q}}(t) + \mathbf{H} \ (\mathbf{q}(t), \dot{\mathbf{q}}(t)) + \mathbf{C} \ (\mathbf{q}(t)) \tag{3.8}$$

The term τ represents the joint torque vector. The terms $\mathbf{q}$, $\dot{\mathbf{q}}$, and $\ddot{\mathbf{q}}$ represent the joint angles, velocities, and accelerations vectors respectively. The inertia matrix is represented by $\mathbf{I}$. Coriolis and centrifugal terms are represented by $\mathbf{H}$. $\mathbf{C}$ is the matrix of gravity related terms. As stated in Chapter 2, the Coriolis and centrifugal terms are assumed negligible for this case, and are not considered further.

3.4.2.1 Inertia Tensor The inertia tensor represents the mass and reflected mass effects on each actuator. Because mass is representative of acceleration terms, the inertia tensor represents the interrelated accelerations of one link on the others [15:p 93-96]. For the full six DOF manipulator, the inertia tensor is six-by-six. However, impedance control will be only applied to the first three joints for this thesis. Hence, the inertia tensor of concern will be the upper left three-by-three

sub-tensor identified in Equation 3.9.

$$\left\| \begin{array}{ccc|ccc} \left[\begin{array}{ccc} I_{11} & I_{12} & I_{13} \\ I_{21} & I_{22} & I_{23} \\ I_{31} & I_{32} & I_{33} \end{array} \right] & & & I_{14} & I_{15} & I_{16} \\ & & & I_{24} & I_{25} & I_{26} \\ & & & I_{34} & I_{35} & I_{36} \\ I_{41} & I_{42} & I_{43} & I_{44} & I_{45} & I_{46} \\ I_{51} & I_{52} & I_{53} & I_{54} & I_{55} & I_{56} \\ I_{61} & I_{62} & I_{63} & I_{64} & I_{65} & I_{66} \end{array} \right\| \qquad (3.9)$$

Inertia tensor values are calculated by combining the Denavit-Hartenburg parameters for the PUMA 560 [15] with the symbolic inertia equations worked out by Tarn [41]. Duvall used MACSYMA computer code [14:p 3-18] to reduce the equations prior to implementing them in computer code. For this effort, a similar reduction was performed using Mathematica [48]. Tarn calculated the inertia terms for joints one through three directly, and included the effects of joints four through six as a load on joint three. This method is acceptable because joints four through six are being commanded to remain at zero angle by a separate PD control loop.

3.4.3 Kinematics Kinematics is the study of position and motion of an object relative to some reference. Kinematics does not deal with the effects of forces. In a robotic manipulator, the task generally involves locating and moving an object from some point to another in the workspace. A majority of manipulators are controlled at the primitive level in joint space. However, a majority of tasks are best described and controlled in a cartesian space. The challenge with manipulator kinematics is to understand what joint space motions produce a desired cartesian motion, or which cartesian motions produce the certain joint motion.

The fundamental aspect of kinematics is identifying the different coordinate axes necessary to translate end effector values into the reference frame coordinates. For an 'n' DOF manipulator there can be 'n' different coordinate frames. To provide

a systematic and standardized way of assigning coordinate frames to a manipulator, Denavit and Hartenburg [12, 15] developed a method which is simple and straight forward. On this theme Fu, Gonzalez, and Lee [15] describe a composite of all the separate frame-to-frame rotation matrices as the homogenous transformation or hand matrix. The hand matrix describes the position and orientation of the end effector with respect to the reference frame given specified joint angles and the DH link parameters. This four-by-four matrix is

$$\begin{bmatrix} n_x & s_x & a_x & p_x \\ n_y & s_y & a_y & p_y \\ n_z & s_z & a_z & p_z \\ 0 & 0 & 0 & 1 \end{bmatrix} \qquad (3.10)$$

where n, s, and a are the normal, sliding and approach vectors which are the conventions established to identify the position and orientation of the end-effector [15]. The **nasp** coordinate frame attached to an end effector is shown in Figure 3.5. The hand matrix is used to compute reference (world) frame forces and moments, from **nsap** frame forces and moments.

There are two categories of kinematic concern for robot manipulators [15:p12]: direct or forward, and inverse or back. Direct kinematics determines the position and orientation of the manipulator end-effector given the joint positions and some characteristic geometric parameters for the manipulator. Inverse kinematics is determining the necessary joint positions to obtain a specified cartesian position and orientation. For this thesis the bulk of conversions will employ direct kinematic schemes in order to convert force sensor frame data into the reference world frame coordinates. Currently, inverse dynamics is used to gather position data for graphing. Closely related to position conversions, is the need to determine force-to-torque and cartesian-to-joint space velocities. These conversions are accomplished through the Jacobian and inverse Jacobian matrices.
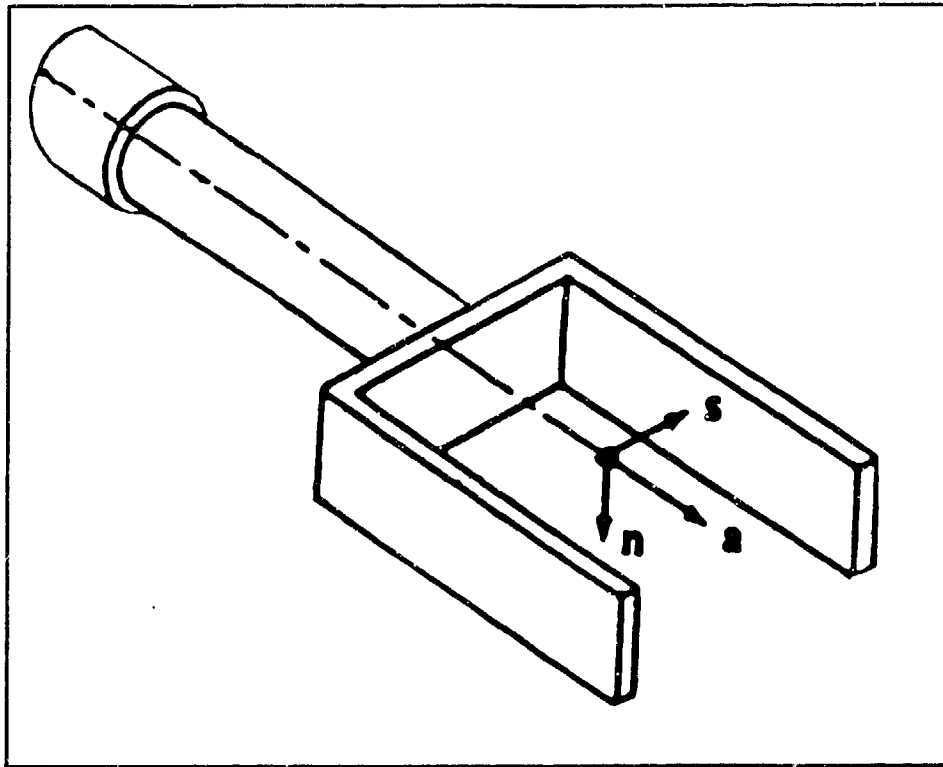
Figure 3.5. Representation of the NSAP Direction [15]

3.4.3.1 Jacobian The Jacobian is described in detail in several references [15, 6, 25] and is based on the relationship between joint and cartesian velocities.

$$\dot{x} = \mathbf{J}\,\dot{q} \qquad (3.11)$$

Derivation of the Jacobian was calculated by taking the derivative of the end effector position vector. This position vector identifies the location of the end-effector origin and is identified in the above hand matrix by the fourth column, the p_i values. Putting the time derivative of the position vector with respect to each of the joint

angles in matrix form produces the three by three Jacobian matrix used in this thesis.

$$
\mathbf{J}(\mathbf{q}) \;=\; \begin{bmatrix} \frac{dp_x}{d\theta_1} & \frac{dp_x}{d\theta_2} & \frac{dp_x}{d\theta_3} \\[1em] \frac{dp_y}{d\theta_1} & \frac{dp_y}{d\theta_2} & \frac{dp_y}{d\theta_3} \\[1em] \frac{dp_z}{d\theta_1} & \frac{dp_z}{d\theta_2} & \frac{dp_z}{d\theta_3} \end{bmatrix} \tag{3.12}
$$

Thus, when the joint angles and velocities are known, the cartesian velocities can be found from Equations 3.12 and 3.11. The inverse Jacobian allows the determination of joint velocities if joint positions and cartesian velocity are known.

$$
\dot{q} = \mathbf{J}^{-1}\dot{x} \tag{3.13}
$$

The Jacobian transpose is used to relate cartesian forces and moments to joint space torques. As noted earlier, the PUMA is controlled at the primitive level by commanding torques to each joint. These torques are then converted to servo motor currents. The trail to converting force sensor values to joint torques begins with the hand matrix which converts forces from sensor frame to world frame forces. These are next converted to joint torques via the Jacobian transpose:

$$
\tau = J^T F \tag{3.14}
$$

Where τ is joint torque vector, J^T is the Jacobian transpose, and F is the cartesian force vector.

3.5 FORTRAN Implementation of the Control Law

The control law was coded in to VMS FORTRAN using the kinematic relationships and the Jacobian described above, along with the diagonal M, B, and K matrices. A complete listing of selected FORTRAN programs can be found in [2].

3.5.1 Feedforward Gravity For a serial manipulator like the PUMA, the axis of rotation for the two heavy links is perpendicular to the gravity field making these links greatly influenced by gravity. Gravity compensation is accomplished by including a modeled gravity effect as a feedforward term in the compliant controller. Again, the work of Tarn served as a basis for calculations. With its axis co-linear with the gravity field, joint one gravity effects are neglected [41]:

$$
\begin{aligned}
C_1 &= 0.0 \\
C_2 &= C_3 - ga_2 m_3 cos(q_2)) + gm_2[y_2 sin(q_2) - (x_2 + a_2)cos(q_2)] \\
C_3 &= -gm_3[(x_3 + a_3)cos(q_2 + q_3) - z_3 sin(q_2 + q_3)]
\end{aligned}
\tag{3.15}
$$

where:

g is gravity = 9.8 $meters/sec^2$

a_2, a_3 are the Denavit-Hartenburg parameters for links 2 and 3

m_2, m_3 are the masses for links 2 and 3

x_3, z_3, y_2 are the first moments of those axes [14:p3-20]

3.5.2 Feedforward Friction The complicated nature of friction effects and compensation was described in the previous chapter. A description of the type of compensation used in the FARCADE algorithm is now provided. The friction model used for this research was identical to that used by Milholen [34]. Summarizing, Milholen's choice was based on previous studies that identified the complexity of accurate compensation through non-adaptive modeling. That discussion identified two critical elements of a friction compensation scheme for this effort:

Generality Ability to address the most dominant friction effects at the relatively slow task speeds encountered in the compliant refueling environment. These

effects were identified by Milholen as stiction(static), coulomb, and viscous frictions [34].

Simplicity The complexity of implementation must be limited. The total computational time required for friction plus the remaining control law must allow for computations at or below the desired operating frequency.

With these restrictions Milholen used the composite stiction, coulomb, viscous model described by Equation 3.16 and depicted in Figure 2.10.

$$
\tau_f = \begin{cases} \tau_c sgn(\dot{q}) & (|\dot{q}|) > d \\ \tau_c sgn(\tau_m) & (|\dot{q}|) \leq d \end{cases} \tag{3.16}
$$

where:

τ_c is the compensation torque (90 % of experimentally determined value for stiction)

sgn($\cdot$) is the function returning the sign of its argument

$\dot{q}$ is the joint velocity in rad/sec

τ_m is the torque supplied to the motor

d is a velocity threshold also determined experimentally

The choice of the switching threshold parameter d was determined by experimentation to be 0.01 [34, 31]. Choosing the sign of τ_m for values less than the threshold is used from the assumption that static friction has overcome motion in this realm.

3.5.3 Non-Impedance Control Implementation of impedance control was applied to three of the six joints of the PUMA manipulator. Joints four through six were controlled by a classical proportional derivative control scheme implemented in joint space. The large assumption of this impedance controller was that the wrist joints were essentially a solid extension of joint three. By commanding the desired

joint positions and velocities to be zero, a form of electronic brake was applied to these joints. The resulting PD control law reduces to

$$\tau = -K_p q - K_v \dot{q} \tag{3.17}$$

Values of K_p and K_v were chosen by Milholen and were not changed here. Duvall [14:3-34] and Milholen [34:3-23] noted that by changing the gains on the PD controlled joints, varying degrees of electronic passive compliance can be achieved. They applied this concept to provide a small degree of compliance in the cartesian 'y' plane by implementing softer gains on joint one.

3.5.4 FARCADE FARCADE is written in VMS FORTRAN and contains all the communication and subroutine calls necessary to operate the PUMA manipulator in impedance mode. It also calls the manipulator and force sensor calibration routines. The impedance controller is actually a sub-routine within FARCADE called MBFC_RT. The following sub-subsection titles represent a FARCADE sub-routine name.

3.5.4.1 MBFC_RT This is where the Jacobians, inertia, M, B, K, gravity, and friction are all combined to create the total torque required for driving the joint motors. MBFC_RT is called each time step calculating new values. These torque values are sent to the coordinator level and then to the PUMA servos. The total torque values are divided into four categories:

Force Torques due to sensed interface forces. Final value obtained by the following combination of the these terms: $-[J^T + I J^{-1} M^{-1}] F_{int}$

Position Torques due to cartesian position errors. Computed from these term: $I J^{-1} M^{-1} K[x_0 - L(q)] + S(q)$.

Velocity Velocity related torques calculated from: $+I J^{-1} M^{-1} B[v_0 - J\dot{q}] + V(\dot{q})$.

Feed-forward Gravity and friction. The gravity term is generally included with the position dependent terms as shown by $S(q)$ above. Friction torque is calculated separately using as a basis Equation 3.16.

3.5.4.2 CARTFOR Employs a two-step process to convert sensed forces to world frame values. First, force sensor calibration bias is removed. Next, these forces are converted to the world frame using the hand matrix. Once converted, these forces are used in MBFC_RT to create the portion of total torque related to interface forces. This routine is also executed each sample period.

3.5.4.3 KIN Calculates the hand matrix each sample period. Once calculated, the values are combined, in MBFC_RT, with forces from CARTFOR. KIN is also used to establish the starting position in the trajectory.

3.6 Summary

This chapter has defined the test environment used in this thesis. The environment consists of computers, a PUMA manipulator, a force sensor, the refueling mock-up, and the software operate and support the environment. The following chapter will set the stage for the actual research performed, by discussing some issues that needed to be resolved prior to full-scale experimentation.

IV. Anomalies

4.1 Overview

During the FORTRAN coding and subsequent 'shakedown' testing of the three DOF impedance control law, three anomalies in the previous two DOF effort were identified. This chapter will explain the anomalies, and the steps taken to correct them.

4.2 Two DOF Impedance Controller

The complex nature of implementing impedance control provides an atmosphere of mistakes and mis-cues. Assuming that all parameters are correct, proceeding from a two DOF impedance controller to a three DOF controller is simply done by expanding the two-by-two matrix form of Equation 2.3. It was during this implementation process, that errors in the previous two DOF FORTRAN code were discovered. The following subsections discuss the data file read error, and the run-time constants.

4.2.1 Data File Read Error
One of the FARCADE subroutines, IMPCONST, reads in data that define the M and B values. These are part of the 'desired' coefficients that make up the second order spring-mass-damper model used to characterize the manipulator impedance. Milholen's implementation of this read routine inverts the order of these terms, effectively making the desired mass term read as the desired damping term and visa versa. Once this read is done the same subroutine creates the constants which are later used in the subroutine MBFC_RT to calculate actual joint torques. All impedance control law calculations done in MBFC_RT rely on the off-line constants created by IMPCONST.

From Equation 2.3, it is evident that the mass matrix used in computing the control law is actually applied in its inverted form; thus in the FORTRAN code M is actually M^{-1}. This mass term is utilized in the force, position, and velocity torque

terms. Any error in mass terms will affect each of these torque terms. The damping term B is used in its un-inverted form, and is used to calculate only the velocity torques.

4.2.2 Run-Time Constants The subroutine, MBFC_RT, is the heart of the impedance calculations. The two DOF version contained constants which were used in the position and velocity torque calculations. These constants have no basis in the theory supporting this control law. The following is a comparison of what the theory states versus what was implemented in the two DOF code:

Theory

$$PositionTorque = I J^{-1} M^{-1} K[x_0 - L(q)] \tag{4.1}$$

$$VelocityTorque = I J^{-1} M^{-1} B[v_0 - J\dot{q}] \tag{4.2}$$

Two DOF FORTRAN Implementation

$$PositionTorque = \widehat{100}(I J^{-1} M^{-1} K[x_0 - L(q)])) \tag{4.3}$$

$$VelocityTorque = I J^{-1} M^{-1} B[v_0 - \widehat{100} J\dot{q}] \tag{4.4}$$

The constant 100 identified by the overbrace is the unsupported term. In a phone conversation with Capt Milholen [35], this constant was discussed. Evidently, the constant value was generated as a result of a trial and error attempt to make the two DOF impedance controller function. After encoding and performing individual subroutine checks, Milholen found that the two DOF controller produced no motion. After several attempts, the above constants provided manipulator motion. The underlying cause for the need to use these constants originates from the IMPCONST data read error.

4.2.3 Implications With these two changes to the two DOF approach, the three DOF implementation was accomplished. Initially all values for desired mass,

damping, and spring constants duplicated the values used by Milholen [34:Table 4.4]. These values are found in Table 4.1.

Table 4.1. Two DOF Assumed Parameters [34:4-13]

Test	Trajectory	ζ	ω_n	M	B	K
T5	Refueling	1.2	7.0	2.041	34.29	100.0

Test runs of the three DOF controller produced extreme instability in the manipulator. Following several attempts to identify the unstable behavior, a study was done to characterize how the two DOF implementation errors changed the second order system model. A summary of the study results follows.

Assuming the desired values as identified by Table 4.1, and evaluating Equation 3.6 based on the transposed read, the following parameters result:

$$\frac{K}{M} = \omega_n^2 = \frac{100}{34.29} = 2.9163$$

$$\frac{B}{M} = 2\zeta\omega_n = \frac{2.041}{34.29} = 0.0595$$

(4.5)

Table 4.2 compares the values for $\frac{K}{M}$ and $\frac{B}{M}$ based on theory, with those shown in Equation 4.5.

Table 4.2. Comparison: Theory vs Two DOF Implementation

Source	ζ	ω_n	M	B	K
Theory	1.2	7.0	2.041	34.29	100.0
2 DOF	0.0174	0.0595	34.29	2.041	100.0

It is clear from this comparison that the values implemented in the two DOF controller varied drastically from what the second order model predicts. These were the values that were being implemented in the control law that Capt Milholen attempted to run prior to adding the constants. From Equations 4.3 and 4.4 an

'effective' value can be obtained by the following:

$$100\frac{K}{M} \quad = \quad \omega_n^2 \quad = \quad 100\frac{100}{34.29} \quad = \quad 291.63$$

(4.6)

$$100\frac{B}{M} \quad = \quad 2\,\zeta\,\omega_n \quad = \quad 100\frac{2.041}{34.29} \quad = \quad 5.950$$

Note that the $\frac{B}{M}$ term assumes that v_0 is small in comparison to $100J\dot{q}$. With the values obtained from these 'effective' spring-mass-damper terms, a final comparison of terms in made in Table 4.3.

Table 4.3. Comparison: Theory, Two DOF Implementation and Effective

Source	ζ	ω_n	M	B	K	σ
Theory	1.2	7.0	2.041	34.29	100	-8.400
2 DOF	0.0174	1.7078	34.29	2.041	100	-0.029
Effective	0.1740	17.078	34.29	204.02	10000	-2.973

Although the choice M, B, and K are arbitrary, they must satisfy the conditions for stability, desired damping, and natural frequency. There is an additional restriction imposed to avoid pole warping which occurs when using a digital system to approximate a continuous one [23, 14, 34]. Equation 4.7 describes this condition.

$$\sigma \geq \frac{-0.1}{T_s}$$

(4.7)

For the current configuration, the sample rate T_s is 5.4 milliseconds. Thus, the additional restriction is found in Equation 4.8.

$$\sigma \geq \frac{-0.1}{T_s} = \frac{-0.1}{5.4 \times 10^{-3}} = -18.52 \; rad/sec$$

(4.8)

Remembering that $\sigma = -\zeta\,\omega_n$, and using the effective values calculated above, the two DOF freedom control law implementation met this criteria, as shown in

Equation 4.9.

$$\sigma = -\zeta \omega_n \geq \frac{-0.1}{T_s}$$
$$-(0.1742)(17.078) = -2.97 \geq -18.52 \, rad/sec \tag{4.9}$$

4.3 Force Errors

During the initial testing of the three DOF controller, it became evident that some of the torque values were incorrect in direction. To isolate the error required several steps. First, to verify the translation of forces from the tool frame to the world frame. Second, assure that the conversion from world forces to joint torques was correct.

4.3.1 Force Conversions: Tool Frame to World Frame

The first area examined was the n_oap kinematic transformation matrix. To test for this type of error, the calculations the transformation matrix were first re-checked. Next, a simulation program was created using the pertinent FARCADE software subroutines and running various arm configurations and fictitious input forces. The goal here was to check for appropriate magnitudes and signs on the resultant forces. During this exercise it was discovered that the force sensor coordinate frame was in error. Following the same convention used in the previous research, it was assumed that the force sensor and world coordinate frames were aligned when the PUMA was in the $(0^o, 90^o, -90^o)$ position. However, in actuality the coordinate frames were aligned in the z and x axes, but were 180° out of phase in the y axis. This situation went undetected by previous researchers because only the x and z force values were used by the two DOF control law. Once discovered, this error was corrected in the appropriate places within the computer code. Force-to-torque checks were done to assure no other conversion errors existed.

4.3.2   Force to Torque Conversion The final area to check for the force related errors was in the conversion from forces to torques. This conversion involves the mass matrix, jacobian transpose, jacobian inverse, and the inertia matrix. Each of these terms was rechecked for theoretical accuracy. None of these terms identified any inaccuracies.

4.4   Joint One Data Corruption

As initial three DOF testing continued, an error in the cartesian 'x' position data was encountered. The same error was evident in the joint one data plots. It was manifest by position spikes as the manipulator traversed the desired trajectory. As the manipulator traveled down the slipway sidewall, the position plots for joints two and three reflected a solid connected line representing actual position. Joint one data, showed spikes that started at the zero position and jumped to some non-zero value. Because the manipulator was physically restrained by the slipway sidewall from returning to zero, it was determined there was some error in the data representing joint one position. When the non-zero endpoints of the position spikes were connected with line segments, the resulting curve represented the actual joint position. This suggested that the joint one data had correct values initially, yet at some point most of that data was being corrupted with zeros. Further investigation of the issue determined that the Assembly level code was somewhere causing the drop-out or corruption of the data. In order to continue research, a temporary fix was implemented. This simple fix reads the values for joint one angles comparing them with the previous values. If the current value is smaller than the previous, the previous value is retained. This is possible to implement because the constraint surface never changes between positive and negative slope on the same run. Figure 4.1 shows the original spiky data with the continuous line resulting from the fix, superimposed on the spikes.
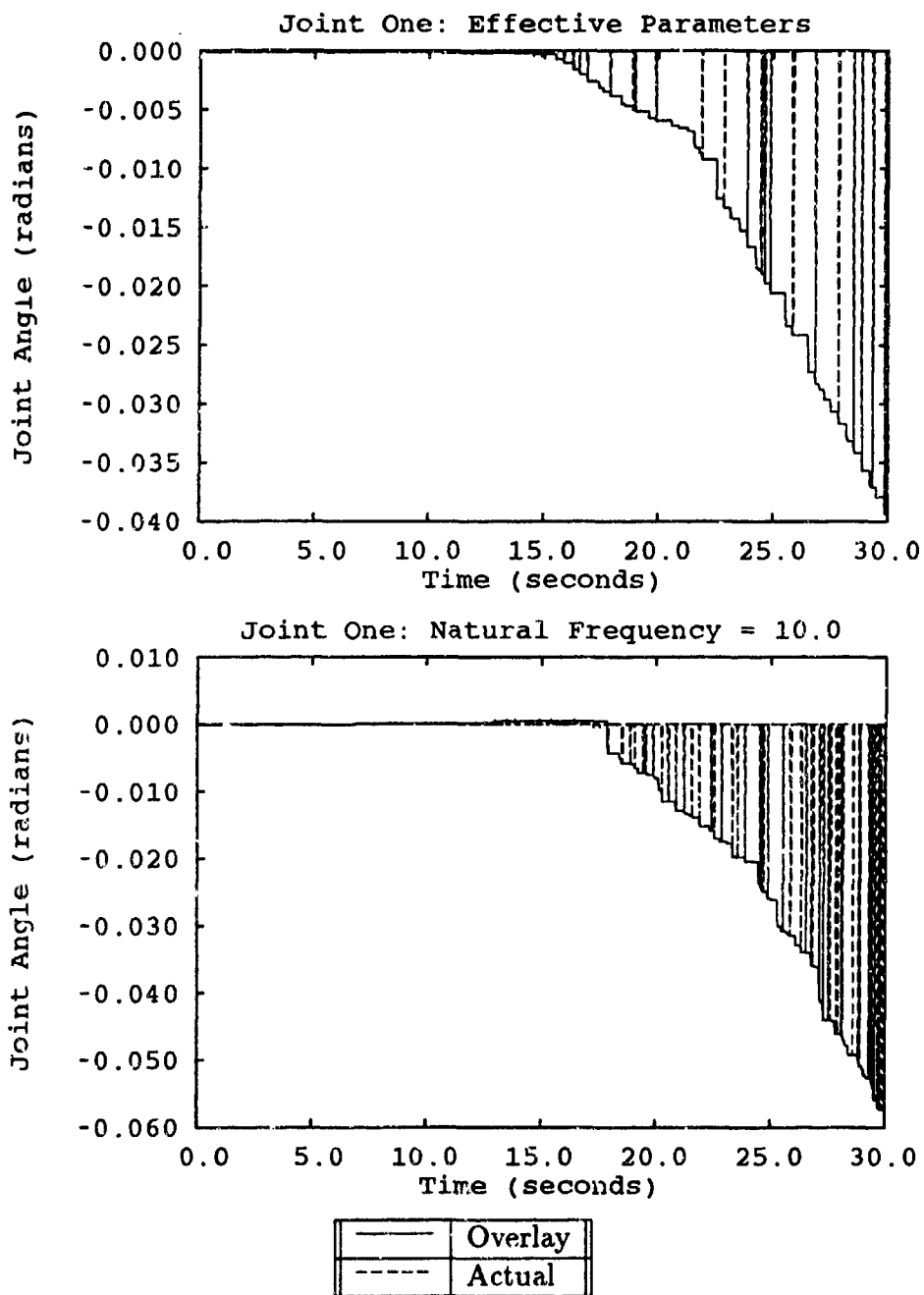
Figure 4.1. Constrained: Joint One Velocity Comparisons

4.5 Summary

This chapter identified the anomalies found in the previous two DOF impedance control implementation. In conjunction, a brief chronology of the changes made to produce a functional two DOF controller was reviewed. The resulting data, found in Table 4.3, summarizes the conditions actually functioning in the two DOF version of impedance control. Next, error in the force related torques required a review of the governing equations used. As a part of that review, the force sensor coordinate frame error was uncovered. Finally, the joint one data corruption issue was revealed, and a fix sufficient to continue testing was implemented. A complete fix will be required for future studies. The following chapter begins evaluating the three DOF impedance controller using the conditions of Table 4.3 as a starting point.

V. Results and Evaluation

5.1 Overview

The previous chapters described the tools needed to create, test and verify a three DOF impedance controller. This chapter presents the details of implementing the three DOF compliant control law. Testing began by applying the effective impedance values used on the two DOF controller, to the current control scheme for three DOF. Three DOF compliance was demonstrated during this phase. Using the two DOF initial parameters as a spring-board, the values for desired mass(M), damping(B), and stiffness(K) in the impedance controller were adjusted in a 'tuning' process to obtain improved performance. Force and velocity filters were applied in order to smooth out the torque profiles. With smoother torque profiles, friction compensation was evaluated.

5.2 Initial Conditions

5.2.1 Trajectory
Once the theory was coded in FORTRAN, the control law was exercised. As a reference point for comparison, the 'effective' values for the previous two DOF control law were applied to the three DOF control law. All tests were performed with the refueling trajectory used by Milholen [34] which is depicted in Figure 5.1. The solid outline represents a side view of the refueling apparatus. The refueling trajectory starts at the world xyz position $(-0.800m, 0.149m, -0.201m)$ then moves in the $-z$ direction to the point $(-0.800m, 0.149m, -0.325m)$. From that point, movement is in the $-x$ direction with termination at $(-1.060m, 0.149m, -0.325m)$. This particular trajectory only requires commanded movement in joints two and three to meet the xz position requirements. Joint one is commanded to remain stationary. Initially this appears to be a limiting case which doesn't exercise all aspects of the three DOF controller. However, because the refueling table is adjustable, the slipway can be set such that
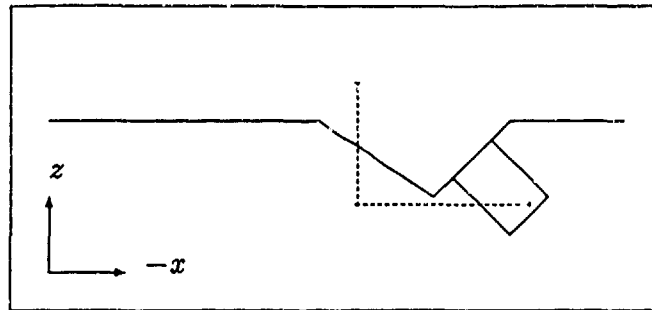
Figure 5.1. Refueling Trajectory [34:4-13]

joint one is deflected from the zero commanded position. The ability to position the physical constraint provides a mechanism to evaluate various degrees of compliant motion. To avoid equipment damage from unstable behavior, each set of conditions was initially performed in free space prior to contact with the refueling table.

5.2.2 Fixture Positioning Due to variations in PUMA calibration, it was not possible to place the refueling table in the same location each time. At times calibration variations would place the manipulator much lower in the z axis direction than others. To accommodate this, the table was adjusted in the x axis direction. Though not as severe, calibration positioning was also inconsistent in the y axis. Therefore, placement of the refueling table in the x and y axis directions was not identical for each test case.

5.2.3 Data Plots All of the data plots presented in this chapter were created by sampling every fifth point out of the original data files. The original data files contained 5555 data points. It was found that plotting out all of the raw points created an extremely difficult plot to analyze. The plots shown in this chapter, contain 1111 data points. A careful comparison of the full data plot with the reduced size revealed no significant degradation in the information portrayed.

5.3 Three DOF Compliance

5.3.1 Verification The first formal phase of testing used the 'effective' parameters found in Table 4.3. Figure 5.2 provides insight into the tracking capability of this parameter set. As expected from Milholen's results, this configuration tracks the desired trajectory quite well. The z axis plot reveals the characteristic stair-step motion which is indicative of stiction. The presence of stiction in this case is possible since the test was made with no friction compensation. Friction compensation is addressed later in the chapter.

The next step was to verify that the three DOF controller could perform two dimensional constrained compliant motion. This task was accomplished by running the trajectory with the refueling platform aligned in the XZ plane. Figure 5.3 represents the torque profile resulting from the two DOF insertion. As expected, the position and total commanded torque were nearly identical for joint one. For this two DOF case, joint one, which corresponds to the y axis direction, did not encounter an obstacle. Joints two and three encountered the slipway causing force and position error in these directions. Figure 5.3 displays the resulting torque profiles quite well.

The small torque on joint one is due to irregularity in the slipway surface combined with slight sensor variations, there was some sensed force in that direction. The data for joints two and three show that as the position torque varies, the force torque responds in the reverse. This is the desirable nature of impedance control. The constant interplay between the position and force torques is what allows compliance to work. Once the two DOF capability was established, all three degrees of freedom were exercised.

5.3.2 Three DOF Compliance This test was set up by placing the refueling platform offset in the plus or minus y direction.Initially, the the nozzle remained parallel to the slipway sidewall. Eventually, the slanted sidewall created an angle whose effect was to increase the position error, similar to placing a wedge along the
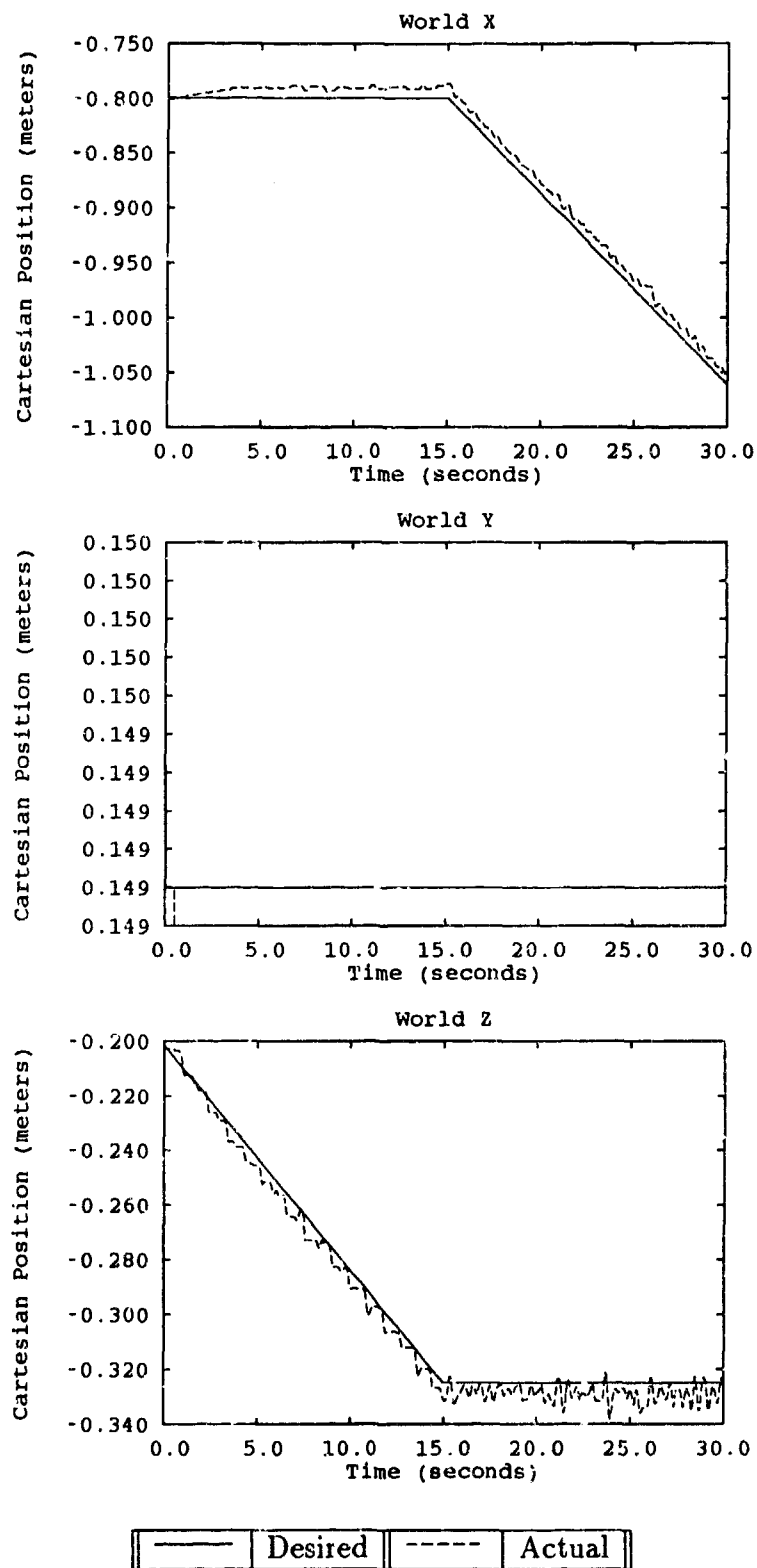
5-3

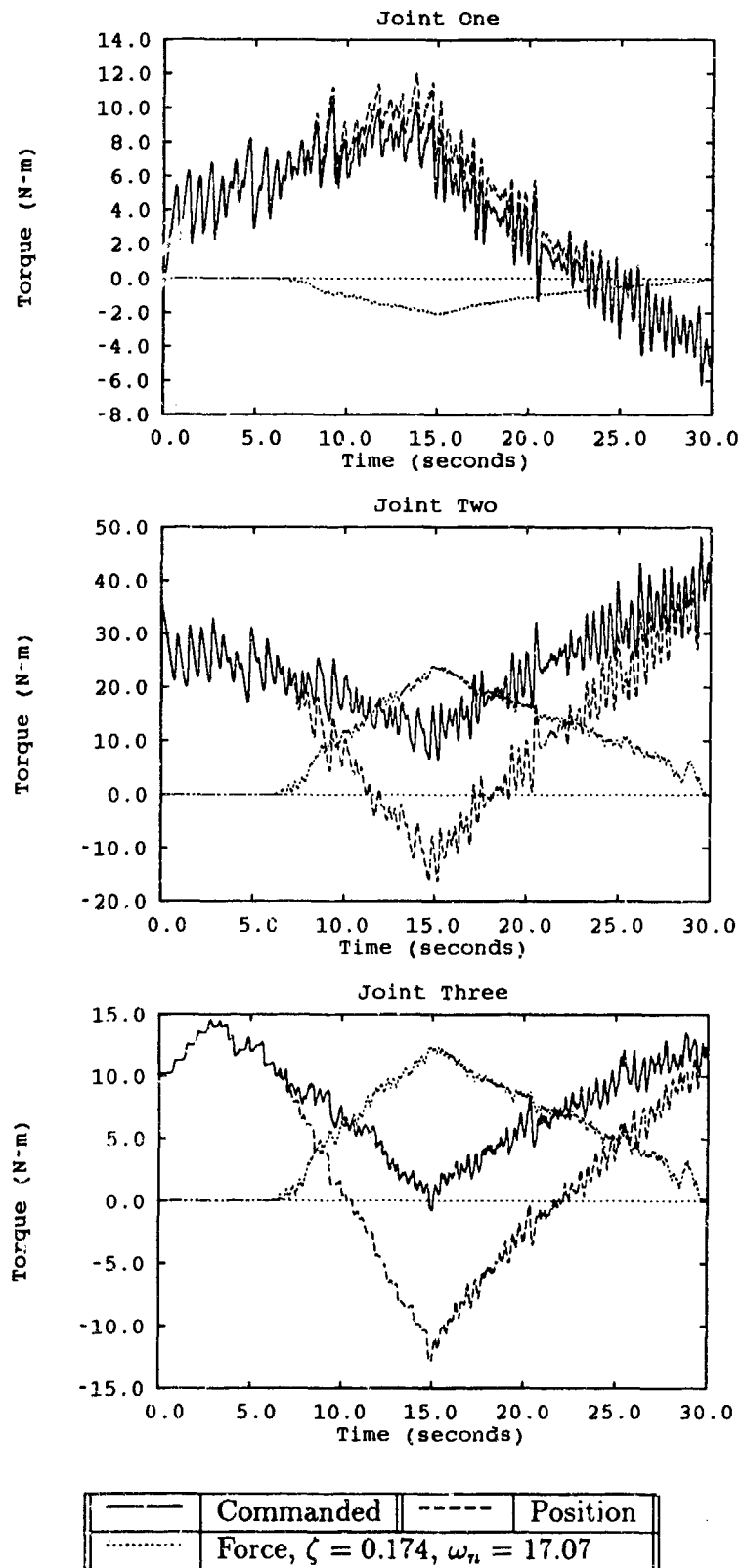Figure 5.2. Freespace: Desired vs Actual Cartesian Trajectory

Figure 5.3. Constrained: Torque Profiles, Effective Parameters XZ Compliance

trajectory, as the manipulator continued in the -x direction.The resultant torque profile is shown in Figure 5.4. The joint one plot clearly shows the mirror nature of force and position torque. This effect is also evident in the other two joint torques.

In addition to verifying compliance in each of the three degrees of freedom, Figure 5.4 reveals some other characteristics. First, the data in the plots for joints two and three is especially rough. The force torques are oscillating at a relatively high frequency. This was the motivation for force filtering which is discussed in a latter section. Additionally, the joint one plot shows that even though the force torque counters the increase in position torque, it only partially nullifies the increase. This means that there was a net increase in total torque in the direction of the sidewall. The physical evidence of this net force was seen by observing slight flexure in the refueling fixture support structure. No damage was done because the support frame is not extremely rigid. This net force issue is discussed in the tuning section.

5.4 'Tuning'

The term tuning here refers to improving performance through variation of the impedance controller second order parameters M, B, and K. Chapter Three described the relation between these parameters and the damping ratio and natural frequency. This section will present the tuning results by actually varying the damping ratio, ζ, the natural frequency, ω_n, and mass.

5.4.1 Damping Ratio
Although the above control law verified compliance in all three directions, the desired parameters created a small damping ratio. Classic control theory suggests that such small values for damping ratio allow for the possibility of overshoot and longer periods of oscillation, which are not desired in impedance control. Figure 5.5 represents the constrained position trajectory plot that results from three different damping ratios. This figure clearly shows that there is little change in trajectory tracking performance between $\zeta = 0.174$ and $\zeta = 1.4$.
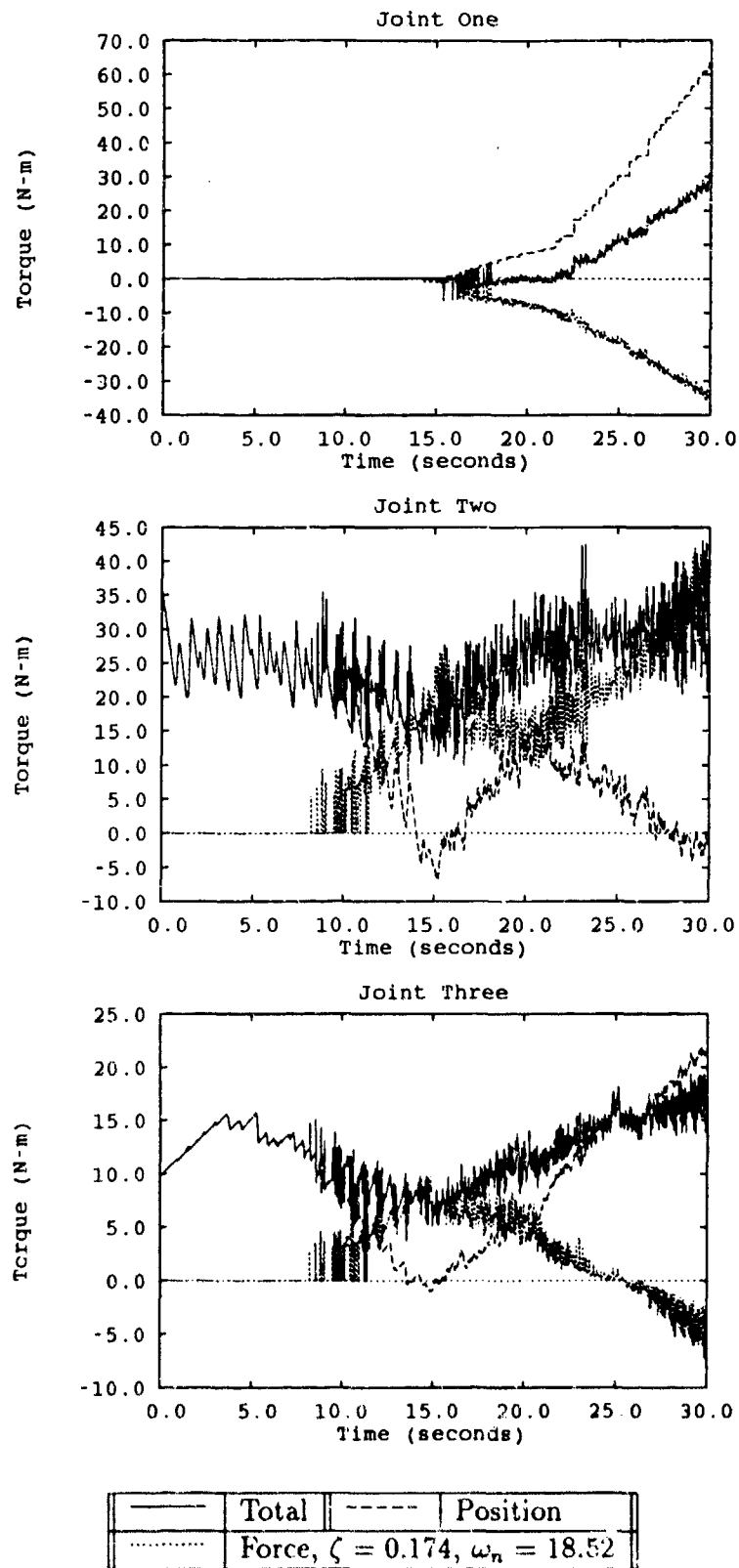
Figure 5.4. Constrained: Torque Profiles, Effective Parameters XYZ Compliance

Figure 5.6, illustrates the torques corresponding to the $\zeta = 1.4$ trajectory plot of Figure 5.5. Comparing Figures 5.5 and 5.6 reveals only a slight variation in the torque profiles for the $\zeta = 0.174$ and the $\zeta = 1.40$ case. The one noticeable feature is the noisier force torques for higher damping ratios.

So far, the only benefit gained from increasing the damping ratio is that the system should theoretically be more stable, not allowing for overshoots and many oscillations. From visual observation the performances are identical. In addition, careful examination of Figure 5.6 reveals that there is an additional amount of higher frequency torque and some spikes that do not correspond to the force terms. Evaluating the velocity torque profiles shows a pattern like that on the total torque line. Figure 5.6 shows the results of increased damping ratio on total torque, as compared to total torque for $\zeta = 0.174$ shown in Figure 5.4. Because damping is directly related to velocity, any increase in the damping ratio will have a similar increase in the magnitude of velocity related torque. In the case where the velocity terms are noisy, increasing the damping will increase that noise. This is the reason velocity filtering will be discussed later in the chapter.

5.4.2 Natural Frequency Variation of the natural frequency, ω_n was done in an attempt to create a better force to position torque balance. As mentioned earlier, the ideal case has the force torque equally matching the position torque arising from the error induced by the obstacle. The natural frequency term is comprised of the square root of the stiffness K divided by the desired mass M. The approach to match torques was accomplished by lowering the position gain. Varying this gain has the effect of changing the natural frequency. Another approach is to choose a desired natural frequency, and find the mass and stiffness combination that will satisfy that condition. Figure 5.7 presents the torque profiles resulting from a natural frequency of 07 radians per second. The point to remember is to evaluate these plots based on the relative change in slope of the torque curves, not on the absolute torque magnitudes. One of the reasons for this is that the desired result is to allow force
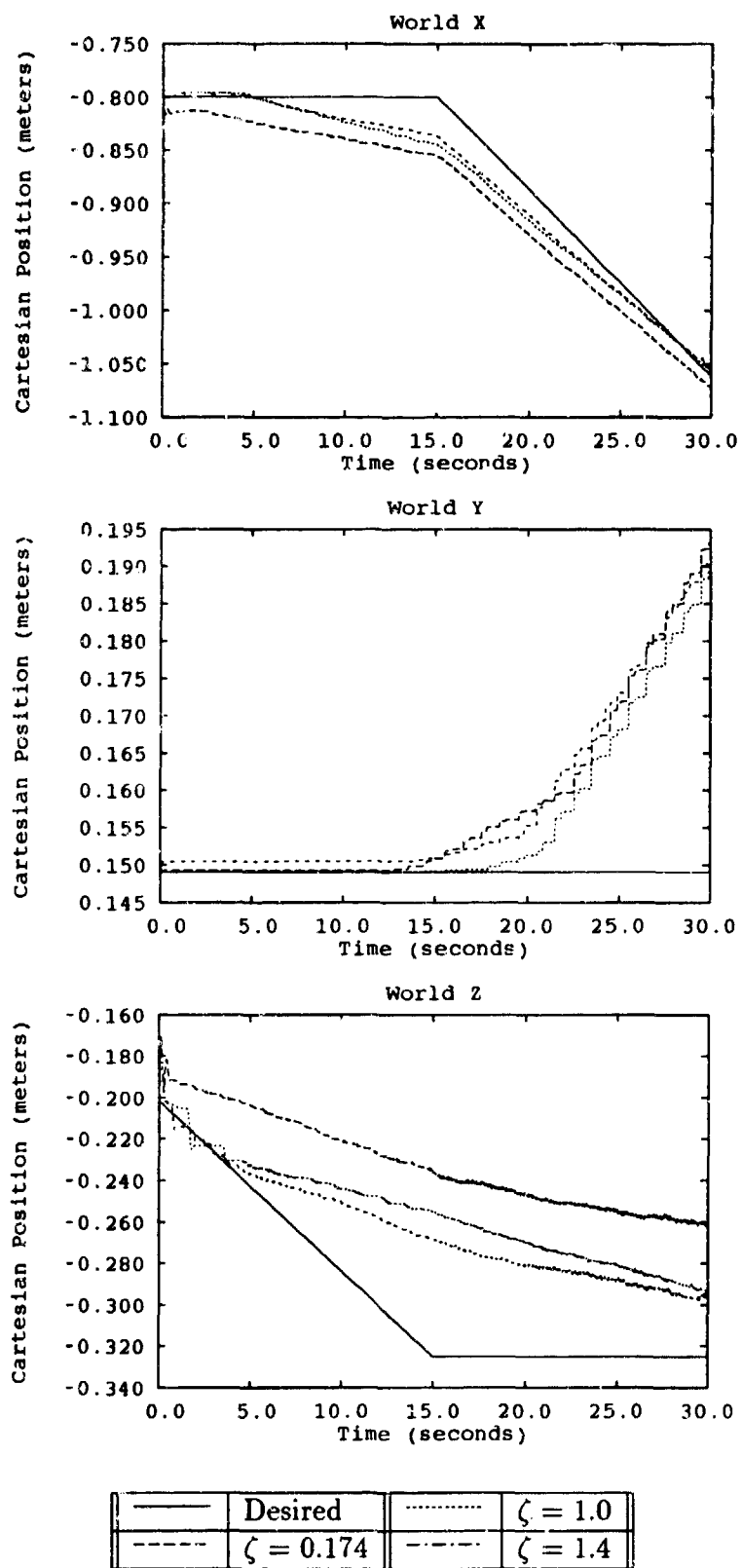
Figure 5.5. Constrained: Comparison of Actual Trajectories at Various ζ Values
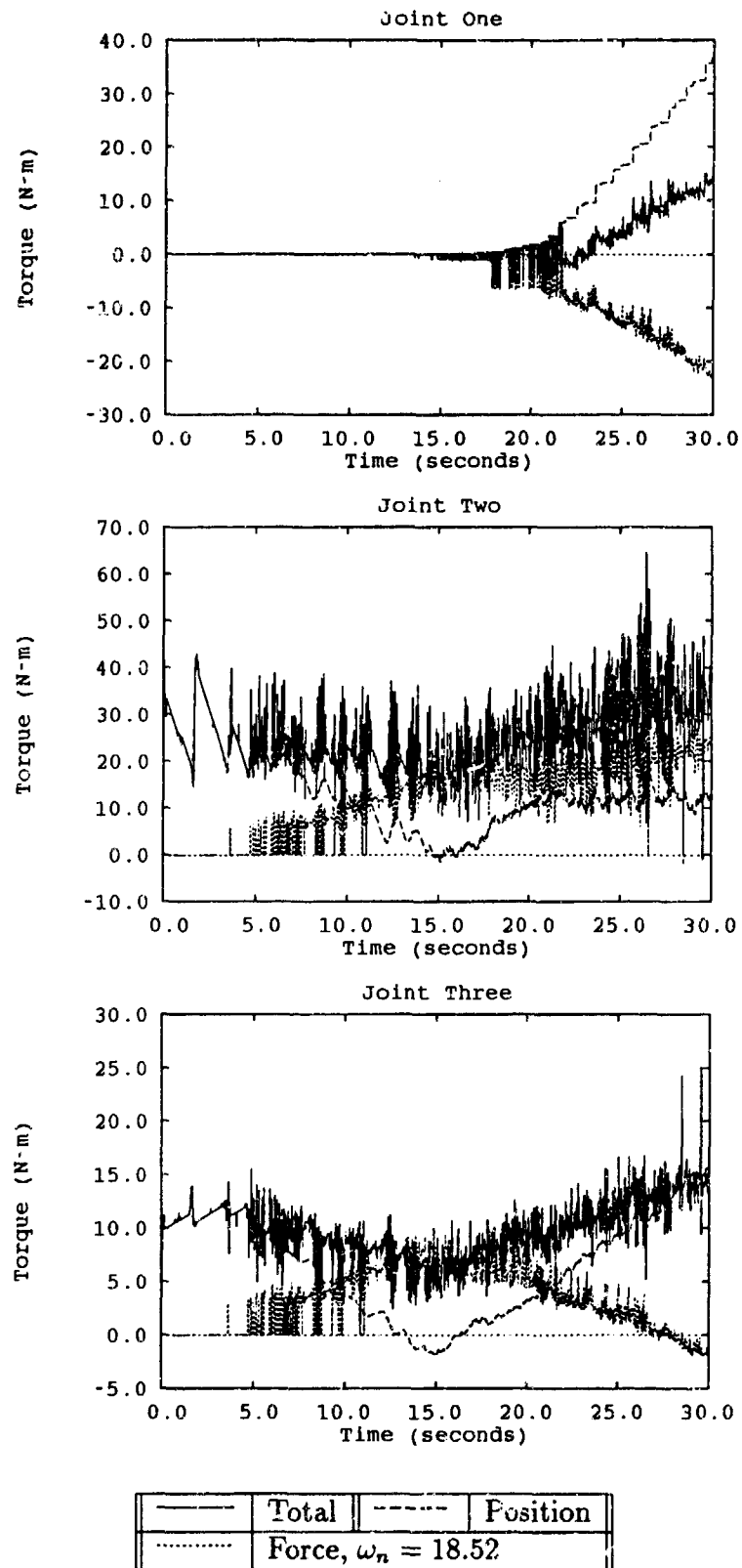
Figure 5.6. Constrained: Torque Profiles, $\zeta = 1.4$

induced torques to nullify the change in position torque due to the error generated from the obstacle. For joint one this means the ideal total torque curve would be flat even when encountering obstacles in that direction. Another reason is that fixture positioning can change the torque magnitude from run to run for the same parameter set.

This exercise demonstrates that the force torque term has more dominance at this frequency, than in the $\omega = 18.52$ case of Figure 5.4. However, the position torque still dominates and causes the total torque slope to increase. Also apparent is the high frequency 'noise' from the force torque. From this exercise, one sees that varying the position gain, i.e. stiffness, does in fact act as a method to reduce the position torque influence.

5.4.3 Mass Another approach to reducing the effect of position torque is similar to the natural frequency approach. Because Hogan's law uses the inverse mass, decreasing the mass term acts to increase the magnitude of the overall term. However, unlike changing the stiffness, in this case varying the mass term affects all of the other torque terms in the controller, i.e. force, velocity, and position torques. Thus, as the mass term is reduced, the torques for force, position, and velocity will each increase in magnitude. Assuming a constant natural frequency, when mass is reduced, the stiffness term must also be reduced to maintain that frequency. A similar effect occurs with the damping torque. On the other hand, decreasing the mass will directly increase the force torque magnitude. The result is an increase in the force torque, with no relative increase in position torque. Figure 5.8 represents torques created by reducing the desired mass from 34.28 kg to 5.0 kg. For joints one and two, changes in the position torque were nearly canceled by the corresponding force torque. This verifies that this method is useful in tuning the manipulator performance.
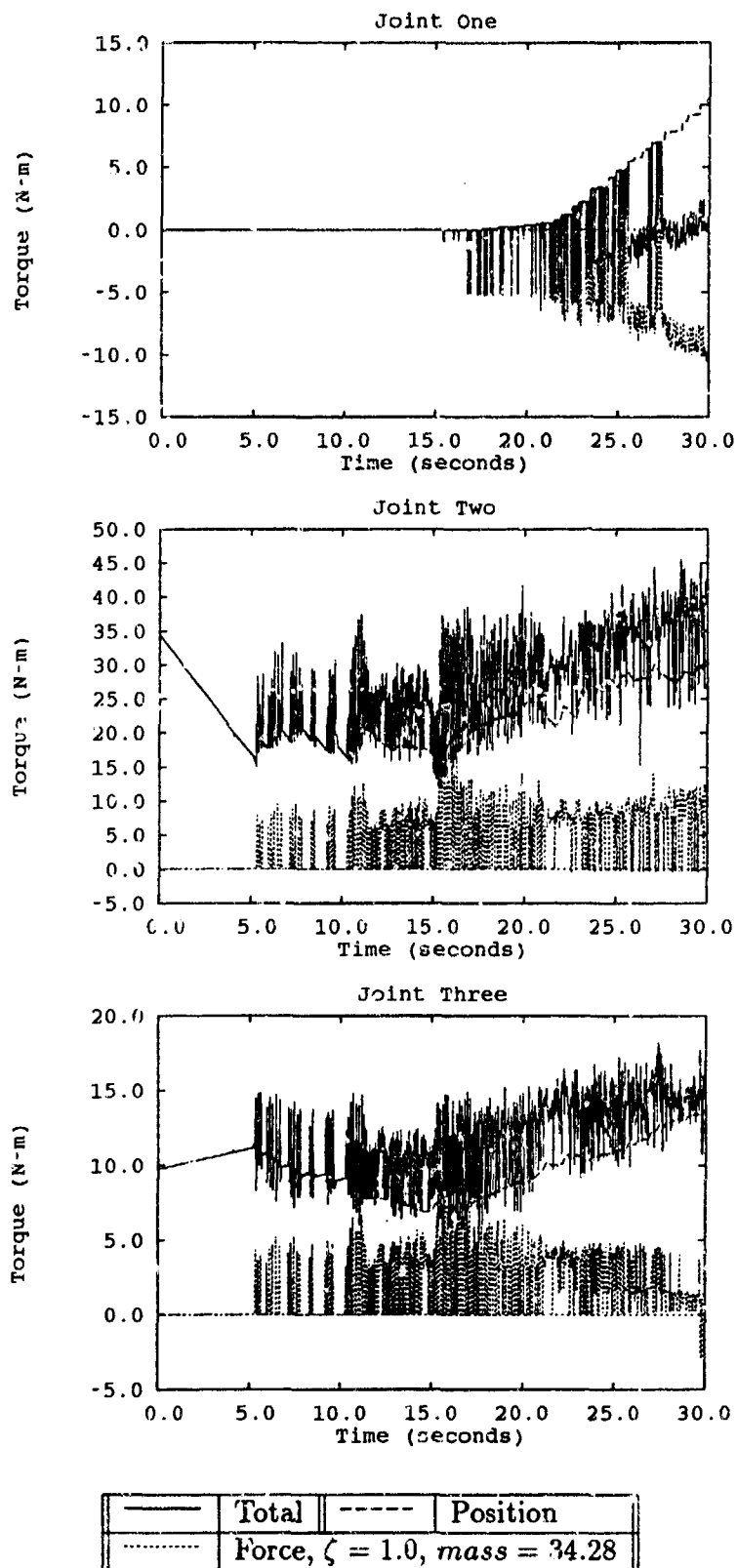
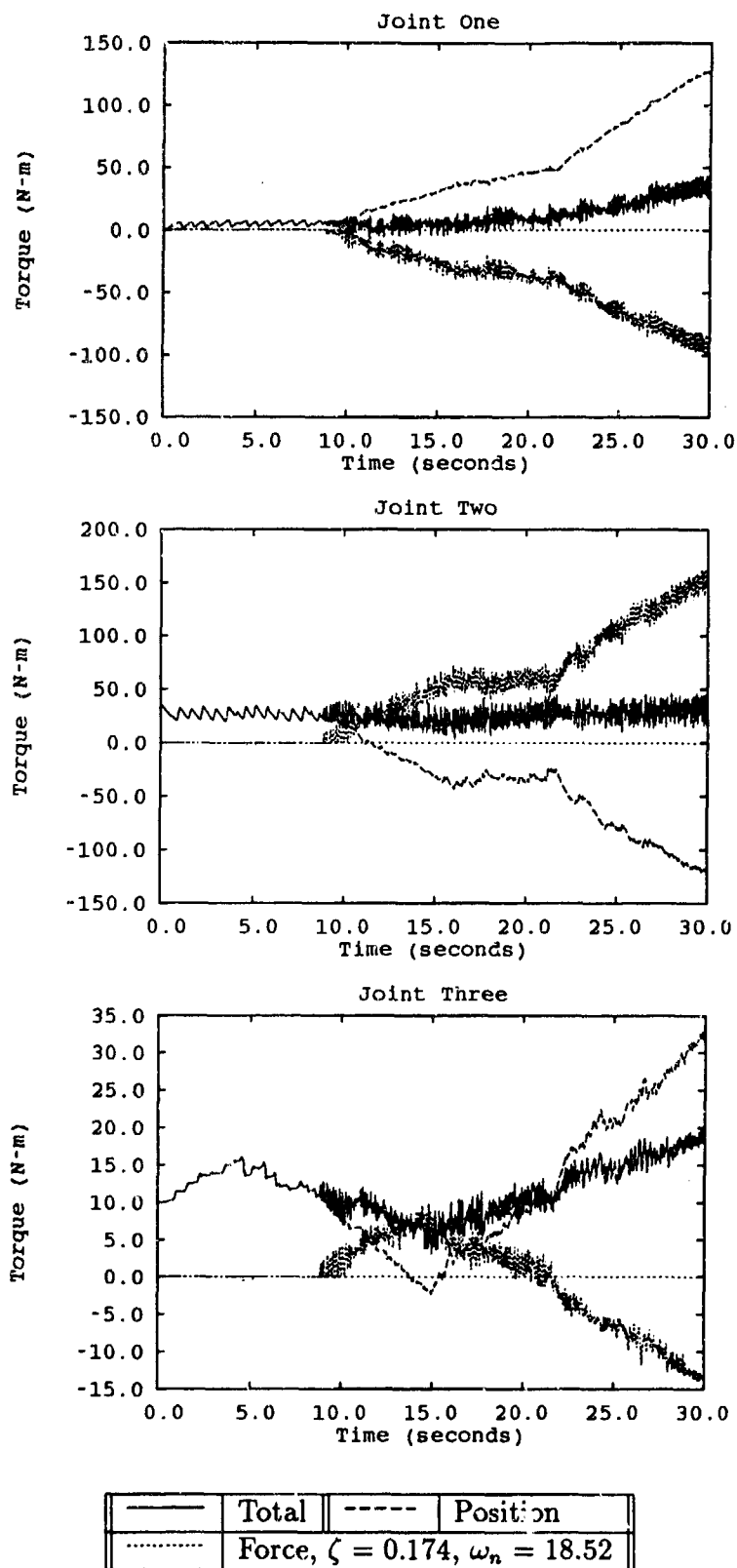Figure 5.7. Constrained: Torques, Reduced $\omega_n = 7$

Figure 5.8. Constrained: Torques, Reduced Mass = 5.0

5.5 Filters

The tuning effort pointed out the higher frequency oscillations and spikes that originated in the force and velocity torques. Both of these terms have important impact on system performance. Because the force portion of impedance is associated with stability, the desired forces and related torques should be as continuous and smooth as possible. Velocity torque is important in two ways. First it relates to the damping characteristics of the controller. Second, the friction compensation model threshold is based on velocity. The sign of the friction torque is obtained from the direction of joint velocity if its greater than the threshold. Otherwise the sign is determined from the position torque.

The filter used for both the force and velocity was very simple: the slope between the current and the previous point is calculated, and compared to a user selected value. If the actual slope is greater than the selected value, the magnitude of the current point is adjusted to meet the imposed slope requirement. Figure 5.9 shows a run without the force filter applied. The force torque has the high frequency oscillations, especially notable in the joints two and three curves. Figure 5.10 shows the torque profile for the same conditions with the force filter applied. There is a definite change in the torque curves due to the filter. However, the velocity torque 'noise' is still present in the total torque.

The velocity filter was applied to the joint space velocities. An example of the velocity torque prior to and after filtering is in Figure 5.11. Figure 5.12 displays the results of velocity filtering on the total torques. It can be seen from these plots, the filter does remove the spikes that were present. This is important because a spike in the torque profile can propagate throughout the entire manipulator and contribute to instabilities.

Joint One

Joint Two

Joint Three

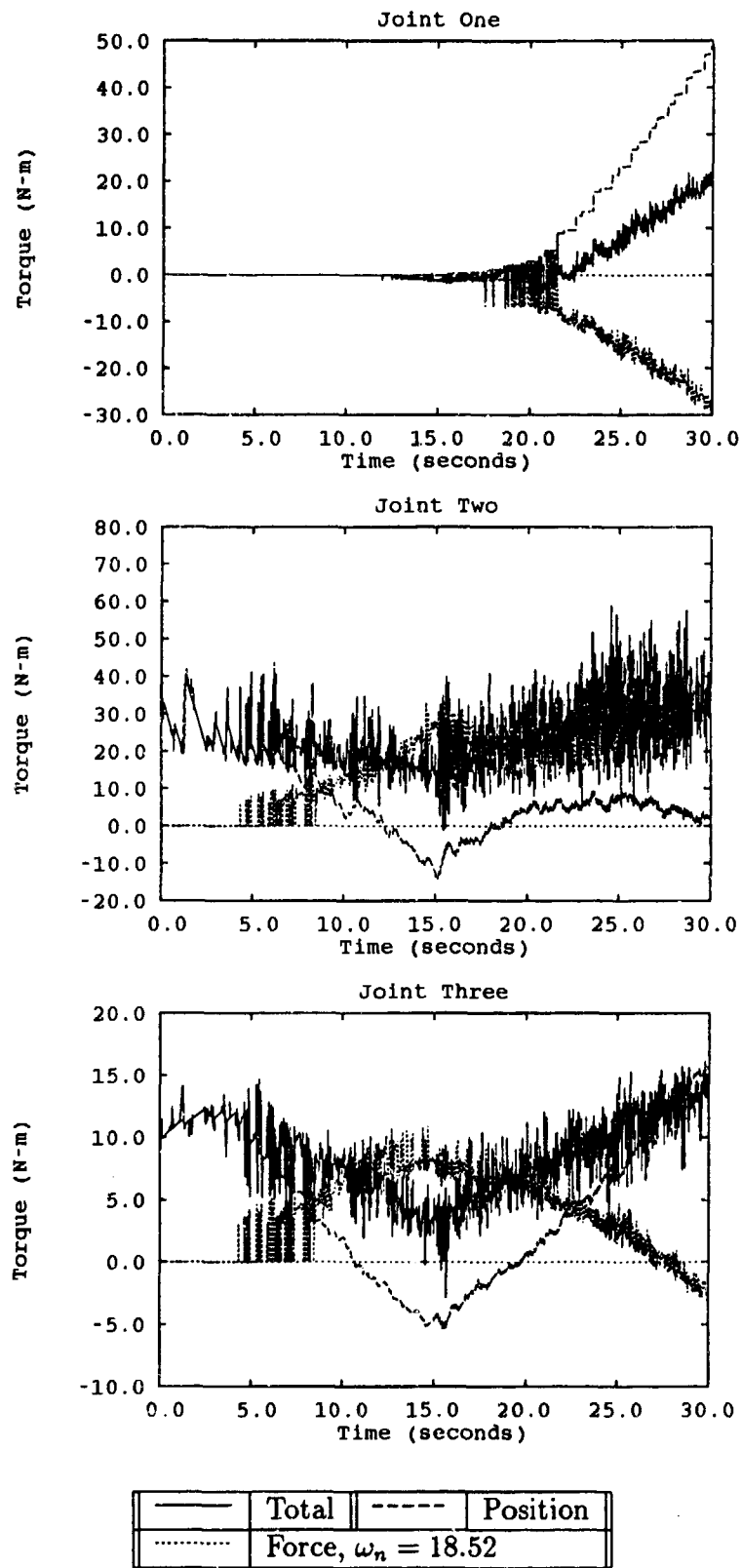|	Total		-----	Position
....	Force, $\omega_n = 18.52$			

Figure 5.9. Constrained: Torque Profiles, $\zeta = 1.2$
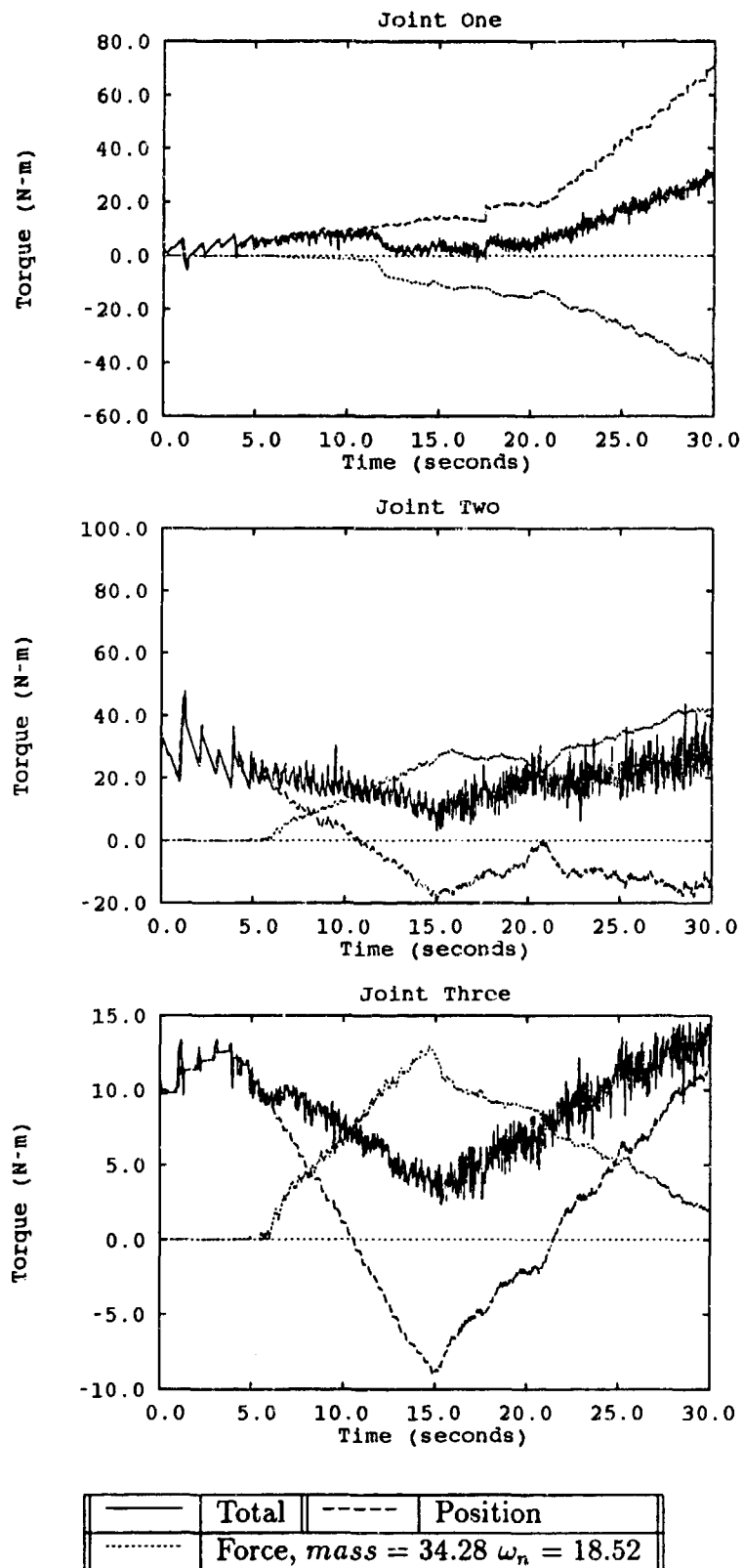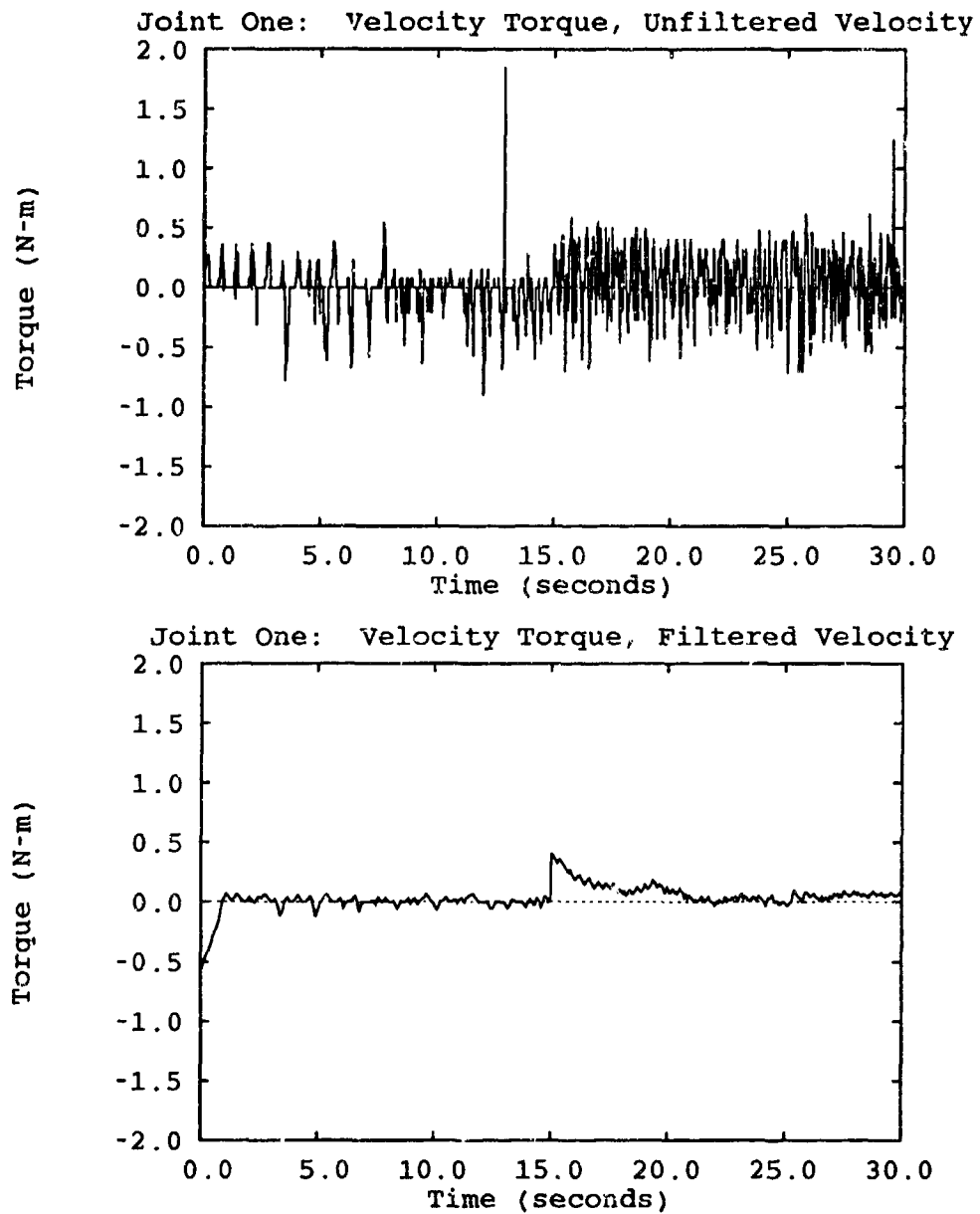
Figure 5.10. Constrained:Torques with Force Filter, $\zeta = 1.2$

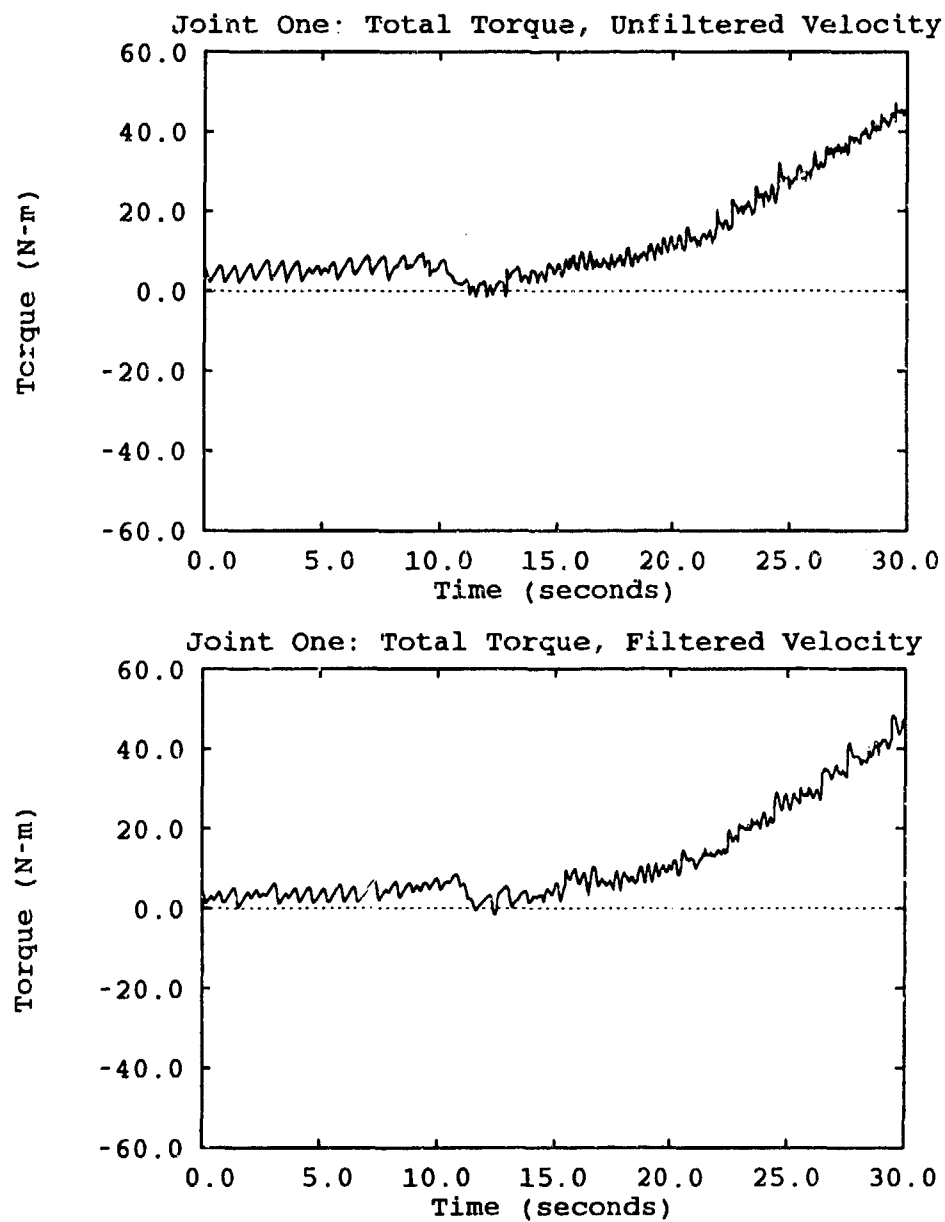Figure 5.11. Constrained: Velocity Torques, $mass = 34.28$kg

Figure 5.12. Constrained: Total Torques, $mass = 34.28$kg

5.6 Friction Compensation

Prior to the temporary fix for joint one data corruption, it was observed that the addition of friction compensation would cause the manipulator to go unstable and enter into limit cycles. One such case is shown in Figure 5.13. The combination of large torque spikes from joint one, and the cyclic switching of the friction torque would combine to create the unstable behavior. After adding the joint one data filter, those types of limit cycles were eliminated. With the force, velocity, and joint one filters in place, an examination of the friction compensation model was performed. Figure 5.14 shows the effect of including the coulomb/viscous friction model described in Chapter Two. The heavy torque bands are due to coulomb friction. These are caused by the direction switching that occurs in this friction model. Comparing this figure to Figure 5.12 reveals that the torque from friction compensation merely adds a torque band to the total torque curve. There is no visual or graphical improvement shown with this compensation included. In fact, from the mechanical view point, such oscillations in the gear train are not desirable. Premature failure because of excessive cycling is possible. In an effort to create a working friction model, the threshold value was changed. In addition, the actual values for coulomb and viscous friction were varied. Neither of these efforts improved the performance for friction compensation. Thus, further testing was performed without friction compensation included.

5.7 Speed

Until now, the testing was done on a thirty second trajectory. This part of the thesis briefly examines whether the impedance controller with similar parameters can accommodate faster motions. The data of Figure 5.15 represents a total time of five seconds to traverse the same trajectory previously covered in thirty seconds. Some re-tuning of the various parameters was required to create a combination that would remain stable. This configuration used a 10 kg mass, a damping ratio of 0.5,
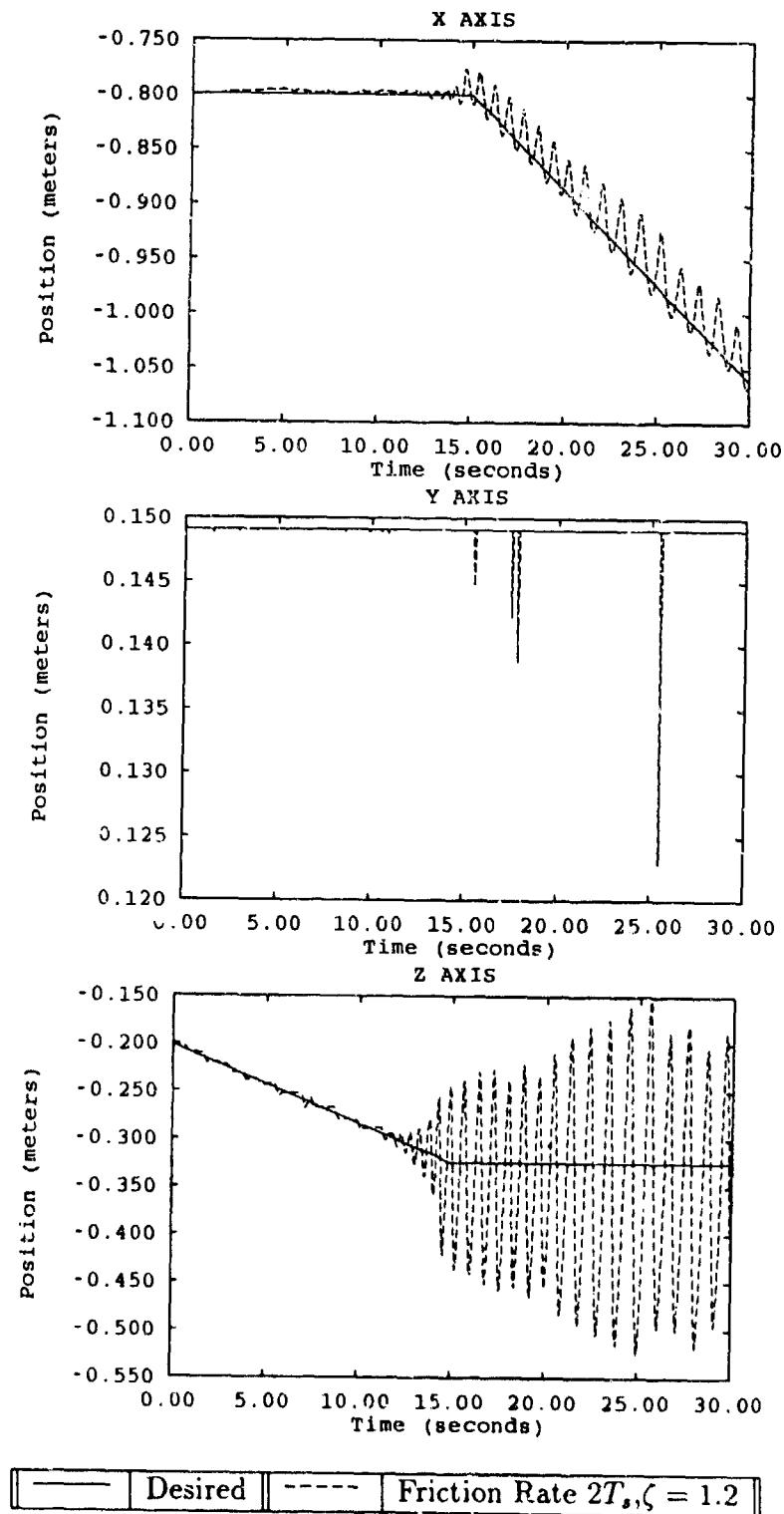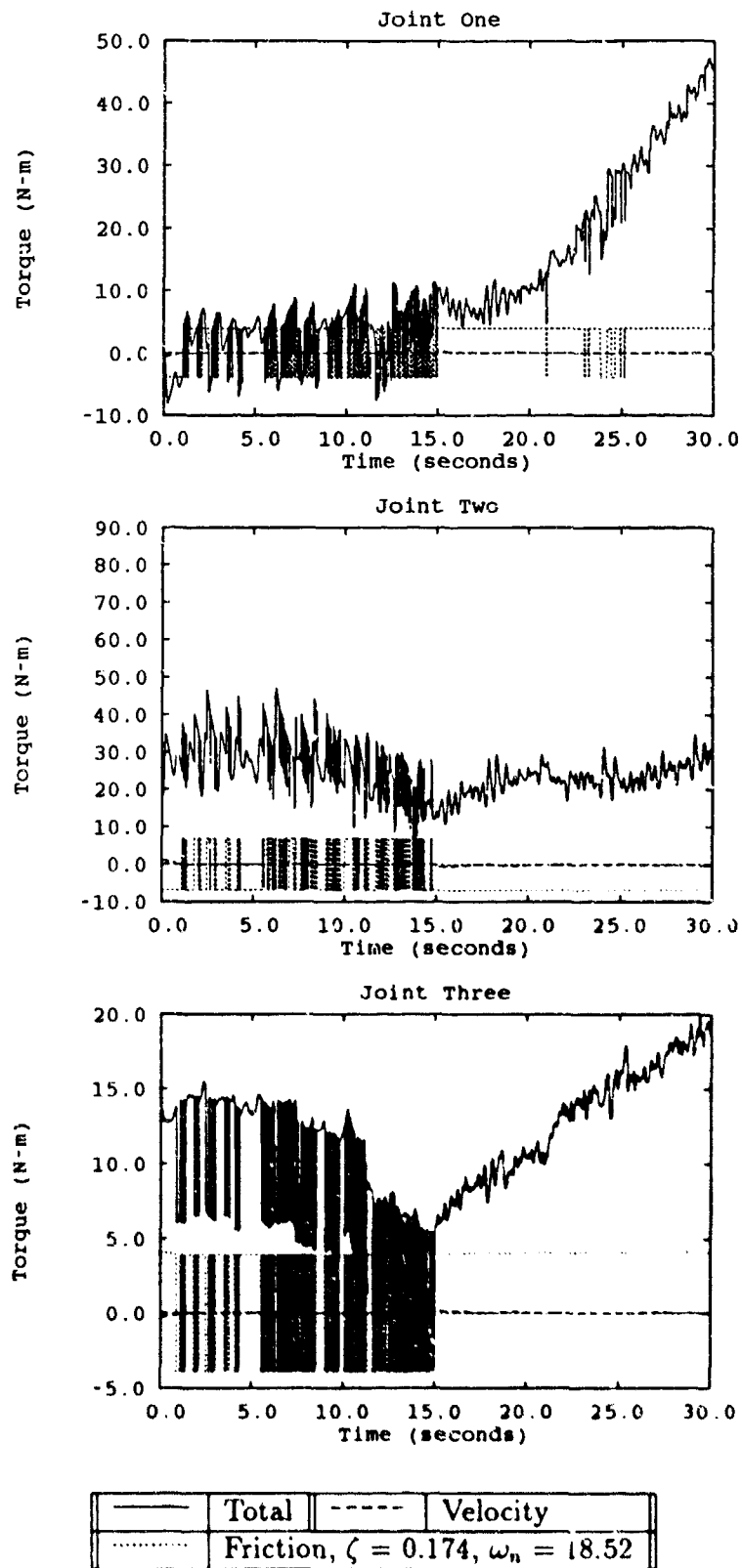
Figure 5.13. Free Space: Limit Cycle

Figure 5.14. Constrained: Torques With Friction Compensation, $mass = 34.28$kg

and a natural frequency of 18.52. Physically, the manipulator followed the side of the slipway in essentially the same manner as previous runs, except six times faster. Visually the performance was identical to the thirty second cases. The shape of the curves in Figure 5.15 appear to be much different than the long runs, but this is expected based on the shortened time frame. This portion of the research identifies that the compliant controller can function well over a broad range of conditions including variations in trajectory speeds.

5.8 Limitations

A final observation about the compliant controller capabilities is made by evaluating the data in Figure 5.16. At the 28 second point there is a large increase in torque magnitudes. That point in the run was where the nozzle contacted the flat portion of the slipway back wall. It was noted in Chapter Three that the mock-up was slightly different in configuration than an actual slipway. This flat back wall was the largest difference. With a discontinuous transition, or corner, between the side wall and the receiver, the axis of the nozzle encountered a condition in which the nozzle axis becomes perpendicular to the wall, but off-set in the y direction from the receiver opening, i.e. stuck in a corner. The manipulator was unable to accommodate this obstacle, therefore it remained in that position building up torques until the trajectory time expired. This shows that this controller can not surmount non-linear impedances, yet it will remain stable in that condition.

5.9 Summary

This chapter has demonstrated three DOF compliant refueling with impedance control. Tuning, or varying the second order parameters revealed that this control law can and does function over a wide range of conditions. Filtering of force and velocity terms was used to create a smoother scenario in which to evaluate friction compensation. Friction compensation schemes made little improvement over the
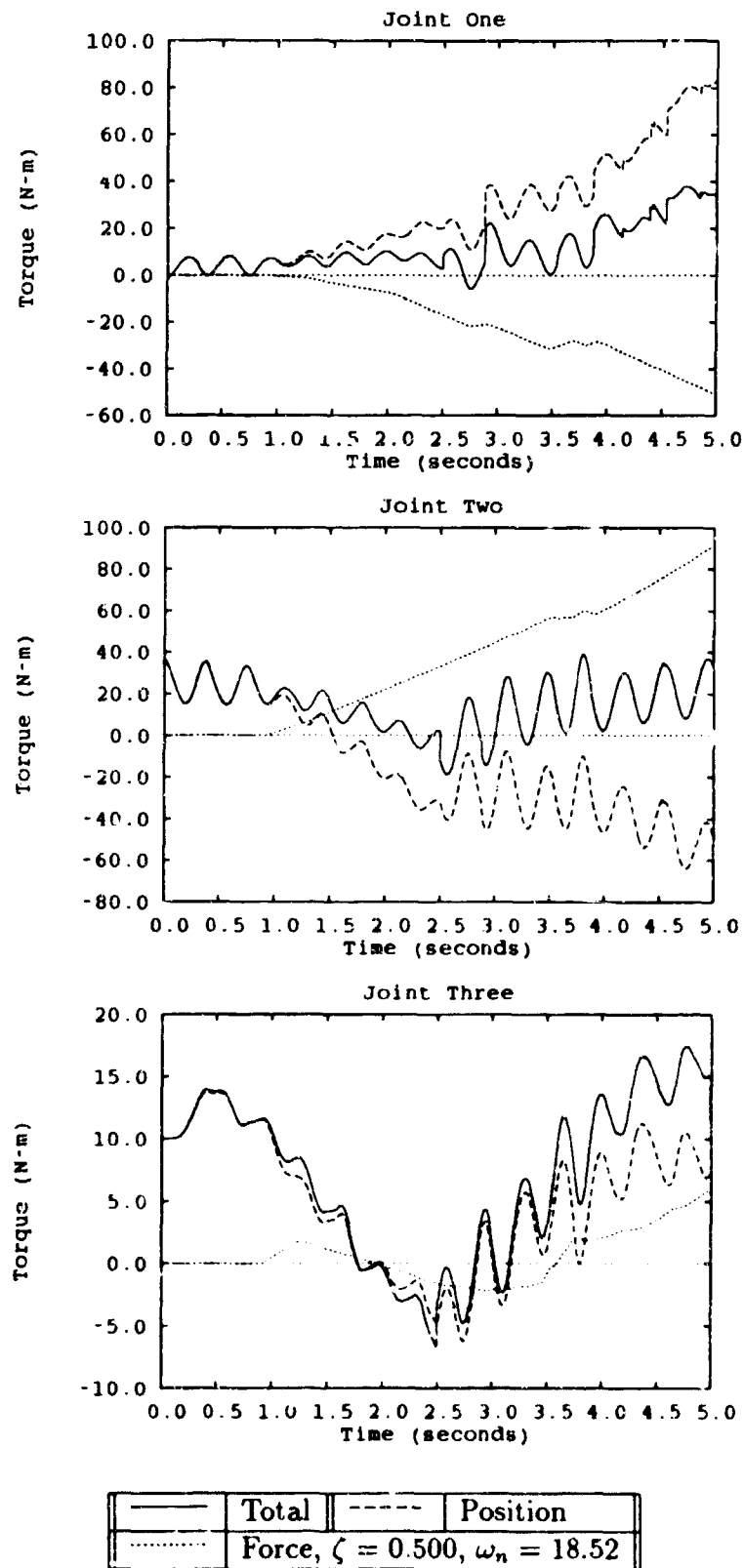
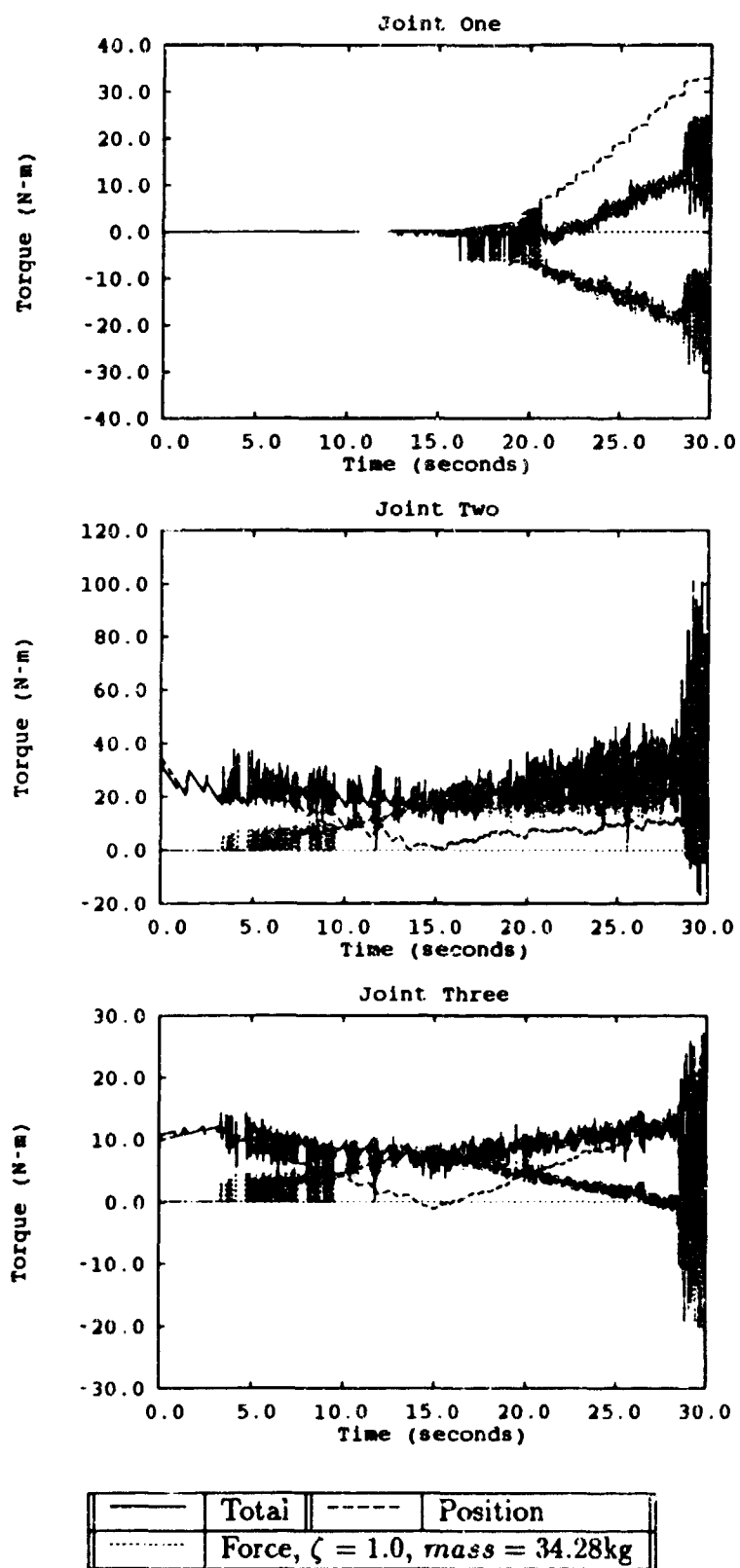Figure 5.15. Constrained: Torques, High Speed, *mass* = 10.00kg

Figure 5.16. Constrained: Torques, Reduced $\omega_n = 12$

uncompensated, $\zeta = .174$ case. Data was presented which indicates that impedance control will provide compliance at much higher velocities. Finally, the linear surface tracking limitations of the control law were exposed.

VI. Conclusions and Recommendations

6.1 Conclusions

Three degrees of freedom compliant motion has been proven and demonstrated on the half-scale Universal Aerial Refueling Receptical Slipway Installation mock-up. In addition, this research has provided the following contributions to AFIT compliant motion research:

- Tuning. Impedance parameters can be tuned to achieve desired performance over a wide range of impedance conditions

- Filtering. Simple but effective filtering techniques improved the overall quality of commanded torque. Both force and velocity were filtered.

- Friction Compensation. The current friction model has been shown to provide no performance improvement

The results of this thesis provide, in many ways, a capstone to the AFIT robotics laboratory research in compliant motion. Achieving three DOF capability allows for investigation of a wide range of assembly related tasks. Compliant control can and should be applied in any peg-in-the-hole assembly tasks. Specifically, compliant control should be used in future robotic refueling prototype efforts.

6.2 Recommendations

Often, research of this kind creates more questions than answers. This thesis is no exception. Perhaps the biggest question remaining is how to improve or smooth the compliant trajectory. The persistent stop-start motion problem is not well posed. Until it is, attempts to compensate for the phenomenon will reach limited success. Preliminary research with adaptive techniques suggests that adaptive friction compensation will provide improved performance over the friction model used.

Additionally, interface forces and their effects may play a large role in creating or impeding a smooth continuous constrained motion.

Another interesting aspect to consider is the need for additional compliant degrees of freedom. What benefits can be derived from a full six degree of freedom manipulation task? Can active and passive compliance be integrated into the same task and perform the refueling demonstration? What are the effects of even higher velocity on the results provided here. That is, can compliant tasks be performed as well at much larger velocity. The following is a summary of recommendations for future research in compliant motion and some of the issues its study has raised:

- resolve joint one data corruption

- identify the nature of the stair-step motion

- investigate using adaptive techniques to reduce or eliminate undesired behavior

- increase to six, the compliant degrees of freedom for the same refueling task

- create more precise ways to assure smooth velocity profiles.

- perform the same test a higher velocities

- perform the refueling demonstration at higher sample rates and velocities

- implement a more rigid fixture which requires the entire compliant nature to be handled by the manipulator

- develop a more precise way to consistently repeat the experimental runs; i.e., upgrade to PUMA calibration routines.

The key to future compliant motion studies is to have clean accurate inputs and more consistent test environment. By providing a repeatable laboratory environment, the effect of slight modifications can be better correlated. Problems such as the joint one data corruption, and PUMA calibration point variations act to cloud other issues such as the jerky stair-step motion.

Bibliography

1. Ahmad,S."Second Order Nonlinear Kinematic Effects and Their Compensation," *Proceedings of the 1985 IEEE International Conference on Robotics and Automation,* pp. 307-314, 1985.

2. Andersen, Clayton M. *Source Code Listing for Three Degree of Freedom Compliant Motion Control for Robotic Aircraft Refueling.* Internal Report ARSL-90-10. AFIT Robotic Systems Laboratory, Department of Electrical and Computer Engineering, Air Force Institute of Technology, Wright-Patterson AFB, OH., December 1990.

3. Asada, H. and K. Ogawa."On the Analysis of a Manipulator and its End Effector Interacting with the Environment," *Proceedings of the 1987 IEEE International Conference on Robotics and Automation,* Vol 2, pp.751-756, 1987.

4. Armstrong, B. "Friction: Experimental Determination, Modeling and Compensation," *Proceedings of the 1988 IEEE International Conference on Robotics and Automation,* Vol 3, pp. 1422-1427, 1988.

5. Armstrong-Helouvry, B. "Stick-Slip Arising form Stribeck Friction," *Proceedings of the 1990 IEEE International Conference on Robotics and Automation,* Vol 2, pp. 1377-1382, 1990.

6. Asada, H. and J.-J. Slotine. *Robot Control and Analysis.* New York: John Wiley and Sons, 1986.

7. Bennett, Richard A. *Brightness Invariant Port Recognition for Robotic Aircraft Refueling.* MS Thesis, AFIT/GE/ENG/90D-04. Air Force Institute of Technology, Air University, December 1990.

8. Canudas, C., K.J. Astrom and K. Braun "Adaptive Friction Compensation in DC Motor Drives", *IEEE Journal of Robotics and Automation,* Vol. RA-3, No 6, Dec 1987

9. Canudas De Wit, C., et.al., "Adaptive Friction Compensation in Robot Manipulators: Low-Velocities", *Proceedings of the 1989 IEEE International Conference on Robotics and Automation,* Vol 3, pp.1352-1357, 1989.

10. Canudas De Wit, C. and V. Seront. "Robust Adaptive Friction Compensation," *Proceedings of the 1990 IEEE International Conference on Robotics and Automation,* Vol 2, pp.1383-1388, 1990.

11. D'Azzo, J.J., and C.H. Houpis. *Linear Control System Analysis and Design, Conventional and Modern* New York:McGraw-Hill Book Company, 1981.

12. Denavit, J. and R. S. Hartenberg. "A Kinematic Notatoin for Lower-Pair Mechanisms Based on Matrices," *Journal of Applied Mechanics,* Vol 77, pp 215-221, 1955.

13. Dupont, P. "Friction Modeling in Dynamic Robot Simulations," *Proceedings of the 1990 IEEE International Conference on Decision and Control.* Vol 2, pp. 1370-1376, 1990.

14. Duvall, D.J. *Robotic Compliant Motion Control for Aircraft Refueling Applications.* AFIT/GA/ENG/88D-1 Air Force Institute of Technology, Air University, December 1988.

15. Fu, King-Sun, R.C. Gonzalez, and C.S.G.Lee. *Robotics: Control, Sensing, Vision, and Intelligence.* New York: McGraw-Hill Book Company, 1987.

16. Gilbart J.W. and G.C. Winston. "Adaptive Compensation for an Optical Tracking Telescope." Automatica, Vol.10, pp. 125-131,1974

17. Gogoussis, A. and M. Donath, "Coulomb Friction Effects on the Dynamics of Bearings and Transmissions in Precision Robot Mechanisms," *Proceedings of the 1988 International Conference on Robotics and Automation*, Vol. 3, pp. 1440-1446, 1988.

18. Goto, T.,K. Takeyasu and T. Inoyama. " Control Algorithm for Precision Insert Operation Robots," *IEEE Transactions on Systems, Man and Cybernetics,* Vol SMC-10, Number 1, January 1980.

19. Hogan, N. "Impedance Control: An Approach to Manipulation, Part I - Theory," *ASME Journal of Dynamic Systems, Measurement, and Control,* Vol 107, pp. 1-7, March 1985.

20. Hogan, N. "Impedance Control: An Approach to Manipulation, Part II - Implementation," *ASME Journal of Dynamic Systems, Measurement, and Control,* Vol 107 pp. 8-16, March 1985.

21. Hogan, N. "Impedance Control: An Approach to Manipulation, Part III - Applications," *ASME Journal of Dynamic Systems, Measurement, and Control,* Vol 107 pp. 17-24, March 1985.

22. Hogan, N., "Stable Execution of Contact Tasks Using Impedance Control," *Proceedings of the 1987 IEEE International Conference on Robotics and Automation.* Vol 2, pp.1047-1054, 1987.

23. Houpis, C.H. and G.B. Lamont. *Digital Control Systems.* New York:McGraw-Hill Book Company, 1985.

24. Kazerooni, H. "Robust, Non Linear Impedance Control forRobotic Manipulators," *1989 IEEE Conference on Robotics and Automation* Vol. 2 pp. 741-750.

25. Klafter, R. et.al., *ROBOTIC ENGINEERING an Integrated Approach.* New Jersey: Prentice Hall, 1989.

26. Leahy, M.B. Jr. *The RAL Hierarchial Control System User's Guide, Version 1.0.* Internal Report No. RAL-67. Robotics and Automation Laboratory, Dept of Electrical, Computer and Systems Engineering, Rensselarer Polytechnic Institute, Troy NY, April, 1986.

27. Leahy, M.B. Jr., *Private Communications*, AFIT, April, 1989.

28. Leahy, M.B., Jr., *Experimental Analysis of Model-Based PUMA Robot Control.* AFIT Internal Report No. ARSL-89-3. AFIT Robotic Systems Laboratory, Department of Electrical and Computer Engineering, Air Force Institute of Technology, Wright-Patterson AFB, OH., July 1989.

29. Leahy, M.B. and G.N.Saridis, "Compensation of Unmodeled PUMA Manipulator Dynamics" *1987 IEEE Conference on Robotics and Automation*, Vol 1, pp.151-156, 1987.

30. Leahy, M.B. and G.N.Saridis, "Compensation of Industrial Manipulator Dynamics" *The International Journal of Robotics Research*,Vol 8, No, 4, pp. 73-84,August 1989.

31. Leahy, M.B. Jr. and K. P. Valvanis, "Dynamics Based Control of Robotic Manipulators." *Intellegent Robotic Systems*, Marcel Dekker Inc., Tzafestas, Editor.

32. Leahy, M.B. Jr., *The RAL Real-Time Robotic Algorithm Exerciser User's Guide, Version 1.0.* Internal Report No. RAL-61. Robotics and Automation Laboratory, Dept of Electrical, Computer and Systems Engineering, Rensselaer Polytechnic Institute, Troy NY, November 1985.

33. Mason, M. "Compliance and Force Control for Computer Controlled Manipulators," *IEEE Transactions on Systems, Man and Cybernetics*, Vol. SMC-11, No. 6, June 1981.

34. Milholen, V.W. *Experimental Evaluation of Impedance Contol for Robotic Aircraft Refueling Applications.* AFIT/GE/ENG/89D-32 Air Force Institute of Technology, Air University, December 1989.

35. Milholen, V.W. *Private Communications*, AFIT, July, 1990.

36. Paul, R.P. "Problems and Research Issues Associated with the Hybrid Control of Force and Displacement," *Proceedings of the 1987 IEEE International Conference on Robotics and Automation.* Vol 3, pp. 1966 1971, 1987.

37. Paul, R.P. and B. Shimano. "Compliance and Control," *Proceedings of the Joint Automatic Control Conference*, pp. 694-699, 1976.

38. Salisbury, J.K.,Jr. "Active Stiffness Control of a Manipulator in Cartesian Coordinates," *Proceedings of the 19th IEEE Conference on Decision and Control*, Vol 1, pp. 95-100, 1980.

39. Sharon, A., N. Hogan, D.E. Hardt, "Controller Design in the Physical Domain." *1989 IEEE Conference on Robotics and Automation*, Vol. 1 pp 552-559, 1989

40. Shipman, R. P., *Visual Servoing for Autonomous Aircraft Refueling.* MS Thesis, AFIT/GE/ENG/89D-48. Air Force Institute of Technology, Air University, December 1989.

41. Tarn, T. J. and A. K. Bejczy. "Dynamic Equations for PUMA 560 Robot Arm," Robotics Laboratory Report SSM-RL-85-02, Department of Systems Science and Mathematics, Washington University; St. Louis , MO, July 1985.

42. Tosunoglu, S. and D. Tesar. "State of the Art in Adaptive Control of Robotic Systems," *IEEE Transactions on Aerospace and Electronic Systems,* Vol 24, No 5, September 1988.

43. Townsend, W.T. and J.K. Salisbury. "The Effect of Coulomb Friction and Stiction on Force Control" *Proceedings of the 1987 IEEE International Conference on Robotics and Automation,* Vol 2, pp. 883-889, 1987.

44. Tustin, A., "The Effects of Backlash and of Speed-Dependent Friction on the Stability of Closed-Cycle Control Systems." *Journal of the Institution of Electrical Engineers,* 94(2A):143-51, 1947.

45. Walrath, C.D. "Adaptive Bearing Friction Compensation Based on Recent Knowledge of Dynamic Friction," Automatica, Vol. 20,No. 6, pp.717-727, 1984.

46. Whitney, D.E. "Historical Perspective and State of the Art in Robot Force Control," *The International Journal of Robotics Research,* Vol 6, No. 1, pp. 3–13. Spring 1987.

47. Whitney, D.E. "Force Feedback Control of Manipulator Fine Motions," *Transactions of the ASME, Journal of Dynamic Systems, Measurement, and Control,* Vol 102, pp.126-133, June 1977.

48. Wolfram, Stephen. *Mathematica: A System for Doing Mathematics by Computer.* Redwood City, CA: Addison-Wesley Publishing Company,Inc.,1988.

Vita

Capt Clayton Mark Andersen was born on November 18, 1959, in Culver City, California. The third of six sons, he spent most of his youth in various parts of the Western United States. In 1977, he graduated from Pocatello High School, Pocatello, Idaho. After attending Brigham Young University for a year, he served a voluntary two-year mission in Brazil with the Church of Jesus Christ of Latter-Day Saints. Upon his return from Brazil, he continued his studies at BYU. On May 7, 1982 he was married to Bonnie Jean Manning in Los Angeles, California. Clayton graduated from BYU in December 1985, with a degree in Mechanical Engineering. Immediately following graduation, he entered Air Force Officer Training School. His first assignment in the Air Force was to the Ballistic Missile Office, Norton AFB, CA. Following three years as a Peacekeeper and Rail Garrison project officer, he entered AFIT to obtain a Master of Science in Aeronautical Engineering. Clayton and Bonnie have four daughters, Michelle Faye, Kimberly Jean, Julie Marie, and Caitlin Eileen.

Permanent address: 1361 Jane St
                            Pocatello, Idaho 83201

REPORT DOCUMENTATION PAGE

Form Approved
OMB No 0704-0188

1. AGENCY USE ONLY (Leave blank)	2. REPORT DATE December 1990	3. REPORT TYPE AND DATES COVERED Master's Thesis

4. TITLE AND SUBTITLE

THREE DEGREES OF FREEDOM COMPLIANT MOTION
CONTROL FOR ROBOTIC AIRCRAFT REFUELING

5. FUNDING NUMBERS

6. AUTHOR(S)

Clayton M. Andersen, Captain, USAF

7. PERFORMING ORGANIZATION NAME(S) AND ADDRESS(ES)

Air Force Institute of Technology
WPAFB OH 45433-6583

8. PERFORMING ORGANIZATION REPORT NUMBER

AFIT/GAE/ENG/90D-01

9. SPONSORING/MONITORING AGENCY NAME(S) AND ADDRESS(ES)

WRDC/FIVMB
WPAFB, OH 45433-6583

10. SPONSORING/MONITORING AGENCY REPORT NUMBER

11. SUPPLEMENTARY NOTES

12a. DISTRIBUTION/AVAILABILITY STATEMENT

Approved for public release; distribution unlimited

12b. DISTRIBUTION CODE

13. ABSTRACT (Maximum 200 words)

The Air Force Institute of Technology(AFIT) supports on-going research in application of robotic technology to enhance assembly tasks. As a testbed, AFIT supports the ground-based aerial refueling project, with an emphasis on visual servoing techniques and compliant motion control. This thesis focuses on compliant motion control. Previous research developed the testing environment, which includes a PUMA-560 industrial manipulator, and a half scale mock-up of an aerial refueling system. This effort corrected and expanded the existing two degree of freedom(DOF) compliant controller to three DOF. Three DOF compliance was demonstrated by inserting the refueling nozzle into the receiver port. Tuning, carried out by adjusting desired model variables, characterized the impedance controller to function over a wide range of desired dynamics. In addition, irregular force and velocity torque profiles were attenuated through basic filtering schemes, providing an environment in which friction compensation was tested. Finally, preliminary studies into faster trajectories provide impetus for further study in the area of high speed compliant assembly. The three DOF compliant controller combined with the visual servoing techniques, provides a strong environment to test and evaluate robotic technologies for constrained motion assembly tasks.

14. SUBJECT TERMS	15. NUMBER OF PAGES
impedance control, force control, compliance, compliant motion, aircraft refueling, robotics, cartesian control, dextrous assembly	93
	16. PRICE CODE

17. SECURITY CLASSIFICATION OF REPORT Unclassified	18. SECURITY CLASSIFICATION OF THIS PAGE Unclassified	19. SECURITY CLASSIFICATION OF ABSTRACT Unclassified	20. LIMITATION OF ABSTRACT UL

Standard Form 298 (Rev. 2-89)
Prescribed by ANSI Std. 239-18
298-102